Materials Today Bio 27 (2024) 101122

Contents lists available at ScienceDirect

Materials Today Bio

journal homepage: www.journals.elsevier.com/materials-today-bio

Black phosphorus quantum dot-modified ADSCs as a novel therapeutic for periodontitis bone loss coupling of osteogenesis and osteoimmunomodulation

Yi He [a,b,1], Yuquan Tang [c,1], Binghui Zeng [a,b], Xun Chen [a,b], Linyu Yuan [a,b], Yunyang Lu [a,b], Weidong Du [a,b], Runze Li [a,b], Yaolin Han [a,b], Feilong Deng [a,b,*], Dongsheng Yu [a,b,**], Wei Zhao [a,b,***]

[a] Hospital of Stomatology, Guanghua School of Stomatology, Institute of Stomatological Research, Sun Yat-sen University, Guangzhou 510080, China
[b] Guangdong Provincial Key Laboratory of Stomatology, Sun Yat-sen University, Guangzhou 510080, China
[c] Zhujiang Hospital, Southern Medical University, Guangzhou, 510080, China

ARTICLE INFO

Keywords:
Black phosphorus quantum dots
Adipose-derived mesenchymal stem cells
Alveolar bone defect repair
Osteogenesis
Osteoimmunomodulation
Periodontitis

ABSTRACT

Alveolar bone defect repair remains a persistent clinical challenge for periodontitis treatment. The use of peripheral functional seed cells is a hot topic in periodontitis. Herein, we explored the cellular behaviors and osteogenic ability of adipose-derived mesenchymal stem cells (ADSCs) treated with black phosphorus quantum dots (BPQDs). Additionally, macrophage polarization, osteogenic effects and angiogenesis were investigated through the paracrine pathway regulated by BPQD-modified ADSCs. Our results demonstrated that BPQDs showed good biocompatibility with ADSCs and BPQD-modified ADSCs could improve the bone repair in vivo inflammatory microenvironment by regulating osteogenesis and osteoimmunomodulation. The BPQDs increased the osteogenic differentiation of ADSCs via the Wnt/β-catenin and BMP2/SMAD5/Runx2 signaling pathway. In addition, BPQD-modified ADSCs promoted the osteogenic effect of BMSCs and facilitated the polarization of macrophages from M1 towards M2 phenotype transformation through the paracrine pathway in the periodontitis microenvironment. This strategy provides a novel idea for treatment of alveolar bone defects for periodontitis in the foreseeable future.

1. Introduction

Periodontitis is a chronic, destructive, and inflammatory condition that affects many people and is a crucial cause of tooth loss [1]. The global incidence of periodontitis ranks sixth among the most common diseases, affecting over 4 billion people worldwide, of which approximately 11 % suffer from severe periodontitis, which has become a significant public health burden worldwide [2,3]. Porphyromonas gingivalis (Pg) contributes to periodontitis by functioning as a keystone pathogen [4]. Pg virulence factors, including hemagglutinins, gingipains, fimbriae and especially lipopolysaccharide (LPS) are important in the induction of alveolar bone loss [4]. The continuous inflammatory microenvironment caused by the Pg leads to the absorption and destruction of alveolar bone, leading to tooth loss [2,3]. Reconstructing the periodontal complex is the ultimate goal of clinical periodontitis treatment, and thus alveolar bone defect repair is a crucial procedure [2]. The existing clinical treatment can slow down periodontitis progression, but achieving alveolar bone defect repair in the inflammatory microenvironment still faces enormous difficulties.

Alveolar bone regeneration is a well-orchestrated process that involves a series of complex biological changes, including osteogenic differentiation, osteoimmunomodulation, and angiogenesis [5]. Osteogenic differentiation of mesenchymal stem cells via increasing alkaline phosphatase (ALP) expression, collagen formation, and extracellular

* Corresponding author.
** Corresponding author.
*** Corresponding author. Hospital of Stomatology, Guanghua School of Stomatology, Institute of Stomatological Research, Sun Yat-sen University, Guangzhou 510080, China.
E-mail addresses: dengfl@mail.sysu.edu.cn (F. Deng), yudsh@mail.sysu.edu.cn (D. Yu), zhaowei3@mail.sysu.edu.cn (W. Zhao).
[1] Note: These authors contributed equally to this work.

https://doi.org/10.1016/j.mtbio.2024.101122
Received 26 March 2024; Received in revised form 24 May 2024; Accepted 9 June 2024
Available online 10 June 2024

matrix mineralization are determining factors to the success of the osteogenesis [6,7]. For the last few years, overwhelming evidence has indicated that osteoimmunomodulation also plays a core role in osteogenesis [8–10].Among the various immune cells, macrophages have been identified to be important in the regulation of osteoimmunomodulation through polarizing the phenotype to pro-inflammatory M1 or pro-healing M2 [11,12]. Effectively decreasing macrophages of the M1 phenotype and increasing the activation of M2 macrophage polarization is beneficial for osteogenesis and bone regeneration [13,14]. As another important factor, angiogenesis of endothelial cells facilitates the osteogenic ability of osteoblasts as well as the speed of bone regeneration, especially in the early healing phase [15–17]. Therefore, developing a strategy to accelerate osteogenic differentiation, macrophage M2 polarization, and angiogenesis is beneficial for alveolar bone defect repair in periodontitis.

Human mesenchymal stem cells (MSCs) can be easily obtained from adult tissues such as bone marrow, periodontal ligaments, pulps and adipose tissues, etc., and hold great potential in regenerative medicine because of their good accessibility and multi-potency ability [18]. In particular, adipose-derived mesenchymal stem cells (ADSCs), isolated from the stromal vascular fraction of adipose tissues, have gradually gained attention for developing an alternative strategy to autologous bone graft to replace or repair defective bone tissues due to the following advantages: (1) ADSCs are abundant in adipose tissue and can be obtained in large quantities with minimal trauma in patients, and the extraction process involves few ethical issues; (2) ADSCs possess strong proliferative and immune regulation abilities [19,20]. ADSCs have multidirectional differentiation potential and can differentiate into various types of cells. More importantly, ADSCs are involved in the regulation of important biological processes through the paracrine function pathway, and thus have broad application prospects in regenerative medicine [21,22]. For example, Bhang et al. found that compared with human ADSCs, injection of conditioned mediums (CMs) from ADSCs to an ischemic region in mice could significantly increase endothelial cell growth, endothelial progenitor cell mobilization from bone marrow, and bone marrow cell homing to the ischemic region [22]. Li et al. demonstrated that gelatin methacryloyl (GelMA) loaded with concentrated hypoxic pretreated ADSC CMs could accelerate wound healing and vascular regeneration in aged skin [23]. Nevertheless, the limited osteogenic capacity, natural ability to differentiate into adipocyte, and unclear paracrine function seriously impede the clinical usage of ADSCs in bone regeneration therapy. Therefore, it is worthwhile to develop strategies to modify ADSCs to accelerate osteogenesis in the inflammatory microenvironment via exogenous paracrine signaling.

As nanotechnology advances by leaps and bounds, various nanomaterials have been reported to facilitate the osteogenic differentiation of MSCs, which hold a great potential in bone tissue engineering and development of nanomaterial-based bone regeneration strategies [24,25]. Because of good optical properties, electronic conductivity, biocompatibility, topological features and biodegradability, black phosphorus (BP) nanomaterials and their derivatives have received attention in the field of biomedicine, including for drug delivery, photothermal therapy, photodynamic therapy, bioimaging and cancer treatment [26]. In particular, BP nanomaterials can be degraded into non-toxic phosphate ions under the physiological environment. As a component of bone tissue, phosphate ions are beneficial to in situ mineralization and bone regeneration, so black phosphorus (BP) nanomaterials and their derivatives hold tremendous potential in bone regeneration engineering [27,28]. BP quantum dots (BPQDs) comprise a new pattern of BP nanostructure that was first synthesized via liquid techniques [29], and BPQDs demonstrate unique optical and electronic properties because of the quantum confinement and edge effects [30]. Compared with BP nanosheets, this ultra-small nanomaterial exhibits less cytotoxicity and higher biocompatibility [31]. However, the effect of BPQDs in alveolar bone repair of periodontitis as well as their mechanisms are still unclear.

The current work aimed to explore the role of BPQD-modified ADSCs in alveolar bone defect repair in an inflammatory microenvironment as well as the underlying mechanisms. Here, we demonstrated that BPQDs showed good biocompatibility with ADSCs and BPQD-modified ADSCs could promote bone defect repair in a rat model of a femoral monocortical defect under an inflammatory microenvironment. The BPQD-modified ADSCs could accelerate their osteogenic ability through the Wnt/β-catenin and BMP2/SMAD5/Runx2 signaling pathways. In addition, BPQD-modified ADSCs could facilitate the osteogenic effect of BMSCs and promote the polarization of macrophages from M1 towards M2 phenotype transformation through the paracrine pathway in the periodontitis microenvironment. We believe that our study will help provide a theoretical and experimental basis for alveolar bone defect repair in periodontitis.

2. Materials and methods

2.1. Culture of ADSCs and BMSCs

For ADSC extraction, inguinal adipose tissue of SD rats was cut into pieces, and digested with 0.1 % type I collagenase for 1 h at 37 °C. After collecting with a 100 μm filter and centrifugation, the cells were resuspended with complete medium which contained Dulbecco's modified eagle medium/nutrient mixture F-12 (DMEM/F12, Gibco, USA), 10 % fetal bovine serum (FBS, Capricorn Scientific, Germany), and 1 % penicillin/streptomycin (Gibco). For BMSC extraction, the bones of SD rats were isolated, and the surrounding soft tissues were thoroughly dissected. The marrow cavities of the femur and tibia were flushed with complete medium. The ADSCs and BMSCs were inoculated in 10 cm tissue culture flasks and incubated in an incubator (37 °C and 5 % CO2). Non-attached cells were removed through frequent medium changes after 72 h. The cells were passaged or collected at approximately 70 %–80 % confluence and passages 3–6 were used in subsequent assays.

The ADSC and BMSC phenotype was detected by positive markers (CD44 and CD90) and native markers (CD34 and CD45) using flow cytometry as previously described [6,32]. The ADSCs and BMSCs were stained for CD34, CD45, CD44, and CD90 (Biolegend, USA) with fluorophore-conjugated antibodies at 4 °C for 30 min. The cells were examined by fluorescence-activated cell sorting after washing with PBS. The gating strategy was defined based on IgG isotype control analysis. For osteogenic or adipogenic differentiation examination, osteogenic medium (Cyagen, USA) or adipogenic medium (Cyagen) was used to treat the ADSCs and BMSCs when the cells reached 90 % confluence. Alizarin Red S staining (Cyagen) and oil red O staining (Cyagen) were performed to detect calcified nodules and lipid droplet formation on day 21.

2.2. Synthesis of BPQDs

Through a simple liquid stripping technique involving ultrasonication, BPQDs were prepared by bath sonication of bulk BP powder [33]. In brief, 30 mg of bulk BP powder was dispersed with 25 mL of N-methyl pyrrolidone (NMP). The mixture was sonicated using an ultrasonic cell disruption system for 3 h with a 1200 W sonic probe. Subsequently, the dispersion was sonicated overnight at 300 W in an ice bath. The obtained dispersion was then centrifuged at 7000 rpm for 20 min, and the supernatant containing BPQDs was decanted. The collected solution was then centrifuged at 13,000 rpm for 45 min and then re-suspended in ultrapure water for further use. The BPQDs were characterized by a transmission electron microscope (TEM, JEM-2100, Jeol, Japan). The surface zeta potential and dynamic fluid diameter were determined using dynamic light scattering (DLS, Zetasizer Nano ZSE, Malvern, Britain).

2.3. Preparation of the conditioned mediums (CMs)

ADSCs were inoculated in 6-well plates at 1×10^5, and when the cells reached 70%–80 % confluence, they were treated with 1 μg/ml BPQD complete medium. Complete medium without BPQDs was as a blank control. After culturing for 48 h, the collected culture medium was centrifuged at 1500 rpm for 20 min at 4 °C. The supernatant was collected and then mixed with complete medium at a ratio of 1:1 to prepare the conditioned mediums (CMs) [34]. The RAW 264.7 cells, BMSCs and human umbilical vein endothelial cells (HUVECs) were treated with the CMs in a LPS (50 ng/ml) simulated inflammatory microenvironment. All the CMs were kept at −80 °C until use.

2.4. In vitro cellular behavior examination

The biocompatibility of BPQDs was tested by using live/dead analysis (Bestbio, China), cytoskeletal staining (Beyotime, China) and cell counting kit-8 (CCK-8, Dojindo, Japan) assays. Calcein-AM/PI was used to detect the viability of ADSCs after treatment with different concentrations of BPQDs in 24-well plates. After 72 h, culture medium containing 1:1000 Calcein-AM and 1:4000 PI was added to the ADSCs and incubated for 20 min. Micrographs of the cells were collected using an inverted microscope (Olympus, Japan).

For cytoskeletal staining, the ADSCs were treated with different concentrations of BPQDs in confocal dishes. After 72 h, the cells were fixed with 4 % formaldehyde (Servicebio, Wuhan, China) for 30 min at room temperature. Subsequently, the samples were stained with actin-tracker green solutions (Beyotime, Shanghai, China) at a ratio of 1:100 for 30 min, then the nuclei were stained with 4′,6-diamidino-2-phenylindole (DAPI, Solarbio, Beijing, China). Images of the cells were collected using a laser confocal scanning microscope (LCSM, Zeiss, Germany).

The proliferation ability of ADSCs treated with different concentrations of BPQDs and those of RAW 264.7, BMSCs, and HUVECs cultured with CMs were examined through CCK-8 assay. After seeding 2000 cells in a 96-well plate, 100 μl of DMEM/F12 with 10 % CCK-8 was added to the wells and then incubated at 37 °C for 2 h. The optical density (OD) values were evaluated using a microplate reader (BioTech, USA) at 450 nm.

2.5. Detection of osteogenic differentiation ability

For alkaline phosphatase (ALP) staining and quantification, the ADSCs and BMSCs were stained with a BCIP/NBT ALP staining kit (Beyotime) and ALP assay kit (Jiancheng Bioengineering, China) to quantify the activity of ALP. ADSCs were treated with different concentrations of BPQDs and BMSCs were treated with CMs in a LPS (50 ng/ml) simulated inflammatory microenvironment for 7 days, then the cells were fixed in 4 % paraformaldehyde for 30 min and BCIP/NBT staining solution was applied for 1 h at room temperature to stain ALP. Micrographs of the ALP staining were collected using an inverted microscope (Zeiss, Germany). For ALP quantification, the cells were lysed by using radio-immunoprecipitation assay lysis buffer (RIPA, CWBIO, China) on ice for 30 min. The cell-lysis product was centrifuged for 30 min at 12,000 rpm at 4 °C and the supernatant was collected. Then, the ALP activity was detected according to the manufacturer's instructions and examined at 520 nm using a microplate reader (BioTech).

Alizarin Red S (ARS) staining and quantification were applied to examine the calcified nodule formation. Briefly, after ADSCs were treated with different concentrations of BPQDs or BMSCs were treated with CMs in a LPS simulated inflammatory microenvironment for 14 days, the cells were fixed with 4 % paraformaldehyde for 30 min. Then, ARS solution (Cyagen Biosciences) was applied for 1 h at room temperature. Redundant ARS solution was flushed thoroughly with distilled water. Micrographs of the mineralized nodules were captured using an inverted microscope (Zeiss). The stained samples were incubated with 10 % hexadecylpyridinium chloride (Sigma-Aldrich, USA) for 1 h, then 100 μl reaction solution was transferred into a 96-well plate and then analyzed at 562 nm using a microplate reader (BioTech).

Table 1
RNA Primers applied in this study.

Gene	Primer sequences
COL1	Forward: 5′-GCGTAGCCTACATGGACCAA-3′
	Reverse: 5′-AAGTTCCGGTGTGACTCGTG-3′
OPN	Forward: 5′-AATGCTGTGTCCTCTGAA-3′
	Reverse: 5′-TCGTCATCATCATCGTCAT-3′
Runx2	Forward: 5′-TACTTCGTCAGCATCCTA-3′
	Reverse: 5′-CGTCAACACCATCATTCT-3′
Osteomodulin	Forward: 5′-AGGTTGTGCTAAGGAATG-3′
	Reverse: 5′-GTTGAGTTGCTGAATGTG-3′
OCN	Forward: 5′-CTCACTCTGCTGGCCCTGAC-3′
	Reverse: 5′-CACCTTACTGCCCTCCTGCTTG-3′
β-catenin	Forward: 5′-GGACAAGCCACAGGATTAC-3′
	Reverse: 5′-CAGTCTCATTCCAAGCCATT-3′
GSK3β	Forward: 5′-CCACAGGAAGTCAGTTAC-3′
	Reverse: 5′-CGCAATCGGACTATGTTA-3′
CMYC	Forward: 5′-TATCACCAGCAACAGCAGAG-3′
	Reverse: 5′-CGCAACATAGGACGGAGAG-3′
TCF-7	Forward: 5′-GAAGAAGAGGCGGTCAAG-3′
	Reverse: 5′- GAGCACTGTCATCGGAAG-3′
BMP2	Forward: 5′-GAATCAGAACACAAGTCAGT-3′
	Reverse: 5′-GACCTGCTAATCCTCACA-3′
SMAD5	forward: 5′-CTGCTGTCCAACGTTAATCG-3′
	Reverse: 5′-GAACAAAGATGCTGCTGTCA-3′
CD86	Forward: 5′-CAGCACGGACTTGAACAACC-3′
	Reverse: 5′- CTCCACGGAAACAGCATCTGA-3′
IL6	Forward: 5′-GACAAAGCCAGAGTCCTTCAGA-3′
	Reverse: 5′-TGTGACTCCAGCTTATCTCTTGG-3′
iNOS	Forward: 5′-TCTAGTGAAGCAAAGCCCAACA-3′
	Reverse: 5′-CCTCACATACTGTGGACGGG-3′
CD206	Forward: 5′-TTCAGCTATTGGACGCGAGG-3′
	Reverse: 5′-GAATCTGACACCCAGCGGAA-3′
Arg1	Forward: 5′-GTAGACCCTGGGGAACACTAT-3′
	Reverse: 5′-ATCACCTTGCCAATCCCCAG-3′
IL10	Forward: 5′-GCTGTCATCGATTTCTCCCCT-3′
	Reverse: 5′-GACACCTTGGTCTTGGAGCTTAT-3′
VEGF	Forward: 5′-ACAACAAATGTGAATGCAGACCA-3′
	Reverse: 5′-GAGGCTCCAGGGCATTAGAC-3′
CD31	Forward: 5′-ACGTGCAGTACACGGAAGTT-3′
	Reverse: 5′-GGAGCCTTCCGTTCTAGAGT-3′
ANG1	Forward: 5′-TCTTTGCACTAAAGAAGGTGTTTT-3′
	Reverse: 5′-TTACAGTCCAACCTCCCCCA-3′
GAPDH	Forward: 5′-AACCTGCCAAGTATGATGA-3′
	Reverse: 5′- GGAGTTGCTGTTGAAGTC-3′

2.6. Gene expression analysis

After ADSCs were treated with different concentrations of BPQDs and BMSCs, RAW 264.7, or HUVECs were treated with different CMs in a LPS simulated inflammatory microenvironment, the total mRNA was harvested using RNAzol Reagent (Molecular Research, USA) and reverse transcribed into cDNA using a Reverse Transcription Kit (Takara, Japan). Real-time quantitative PCR (qPCR) was performed for amplification with triplicate 20 μl reaction volume using an Applied Biosystems®QuantStudio Q5 (ThermoFisher Scientific, USA). The primers for each gene are listed in Table 1, and GAPDH was used as the internal control. The experiment was repeated three times and the results were quantitatively analyzed using the $2^{-\Delta\Delta Ct}$ method.

2.7. Western blot assay

After ADSCs were treated with different concentrations of BPQDs and BMSCs or RAW 264.7 were treated with different CMs in a LPS simulated inflammatory microenvironment, the cells were lysed with RIPA lysis buffer (CWBIO) with 1 % phosphatase and 1 % protease inhibitors (CWBIO) on ice for 30 min. Using a BCA protein assay kit (CWBIO), the protein concentration of the samples was tested.

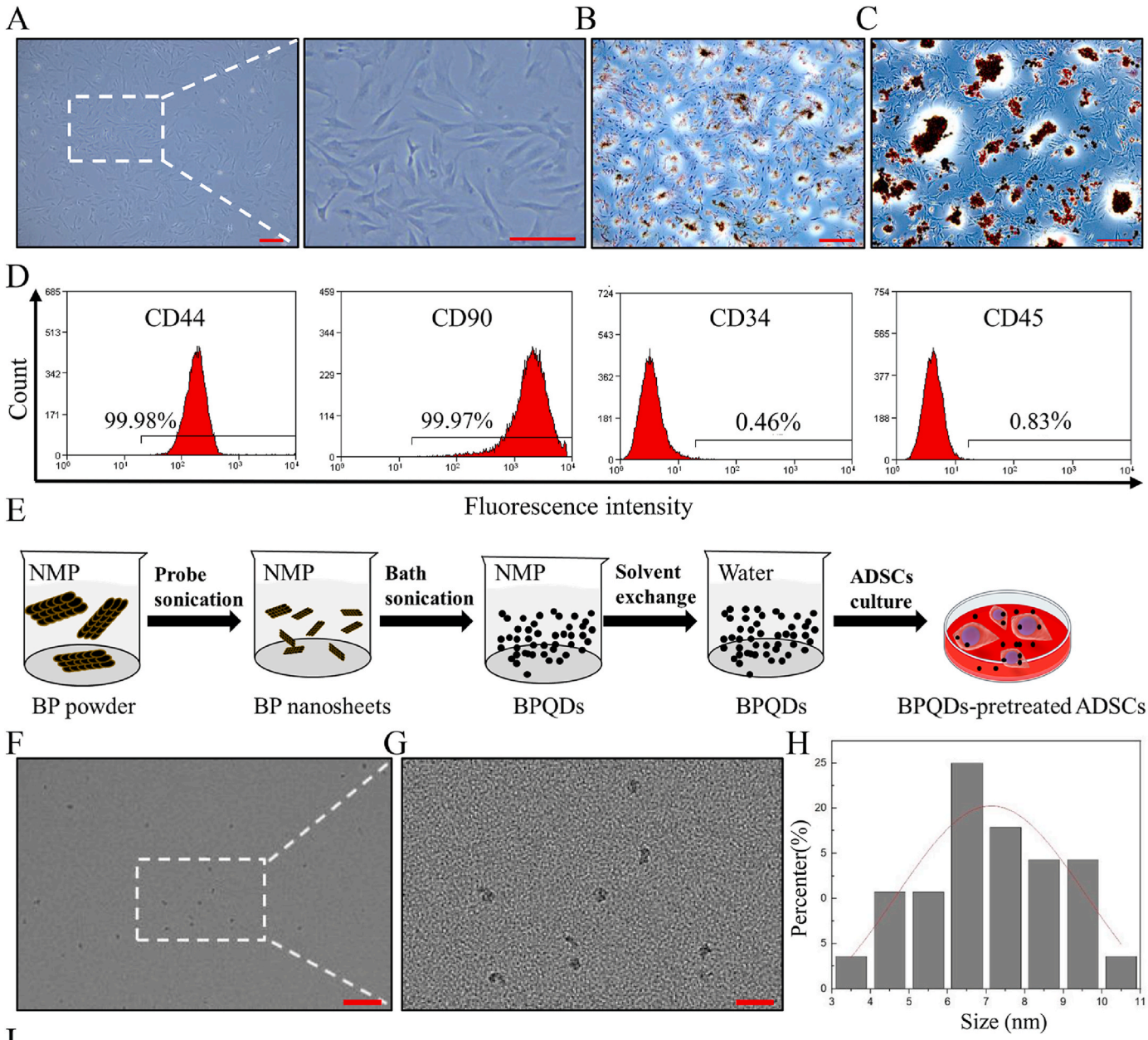

I

Characterization	Condition	Results
Zeta potential	GM	-7.02 ± 1.24 mV
Hydrodynamic size	GM	163.53 ± 18.24 nm

Fig. 1. Characterizations of ADSCs and BPQDs. (A) Typical morphologic characteristics of adherent ADSCs with spindle shapes on a cell culture dish. Scale bar: 200 μm. (B) Alizarin Red staining of ADSCs after osteogenic differentiation treatment. Scale bar: 200 μm. (C) Oil Red O staining of ADSCs after adipogenic differentiation treatment. Scale bar: 200 μm. (D) Immuno-phenotypic marker analysis in ADSCs via flow cytometry. (E) Diagram of BPQD synthesis and ADSC treatment. (F) Representative images (scale bar: 100 nm) and (G) magnified images of BPQDs (scale bar: 300 nm) detected via TEM. (H) Particle size analysis of BPQDs. (I) Zeta potential analysis and hydrodynamic size of BPQDs determined via dynamic light scattering.

Subsequently, 35 μg denatured protein solution was added to SDS-PAGE gels to separate the proteins before transferring to a polyvinylidenefuloride membrane (PVDF, Millipore, USA). The membrane was blocked in 5 % bovine serum albumin (BSA, Sigma-Aldrich) for 1 h at room temperature and then treated with the primary antibodies (Affinity Biosciences, USA) overnight at 4 °C. After incubation with secondary antibodies (Cell signaling, USA) for 1 h, a chemiluminescence kit was applied to examine the immunoblots. ImageJ software was applied to semi-quantitatively analyze the expression of each protein band, and GAPDH or β-actin was applied as an internal loading control.

2.8. Immunofluorescence analysis

After ADSCs were treated with different concentrations of BPQDs

and RAW 264.7 were treated with different CMs in a LPS simulated inflammatory microenvironment, the cells were immobilized with 4 % paraformaldehyde for 30 min, and 0.1 % Triton X-100 (Beyotime) was applied for 10 min at room temperature to permeabilize the cells. After blocking for 30 min in 5 % BSA (Sigma-Aldrich, USA) at room temperature, the primary antibodies (Affinity Biosciences) were added and incubated at 4 °C overnight. Immunofluorescence secondary antibodies (Absmart, China) were added for 1 h to bind to the primary antibody, and then the nuclei were stained with DAPI (Solarbio, China) for 10 min at room temperature. Finally, images of the cells were captured using a LCSM (Zeiss).

2.9. Angiogenesis experiment

For the scratch test, 4×10^5 HUVECs were cultured in 6-well culture plates. When the cells reached 100 % confluence, some cells were removed using a pipette tip and the samples were rinsed with phosphate buffer solution (PBS) to remove excess cells. The samples were then treated with the CMs without FBS in a LPS simulated inflammatory microenvironment. The scratch and remaining cells were captured at 0 and 24 h using an inverted micro-scope (Zeiss) and analyzed using ImageJ.

For the transwell migration analysis, DMEM/F12 was added to the 24-well plate and then 1×10^4 HUVECs or BMSCs were suspended in CMs in the upper chamber of a transwell plate in a LPS simulated inflammatory microenvironment. After 24 h, the cells were treated with 0.1 % crystal violet at room temperature and the cells in the upper chamber were gently removed. After the samples were dried, the stained cells were examined using an inverted microscope (Zeiss). Five random fields were randomly captured, and the average number of migrated cells was counted using ImageJ.

For the tube formation analysis in HUVECs, 50 μL BD Matrigel™ matrix (Sigma-Aldrich) was added to 48-well plates and then placed in a cell incubator until they completely solidified. Then, 3×10^4 HUVECs were suspended with 200 μl FBS-free CMs in a LPS (50 ng/ml) simulated inflammatory microenvironment. Images of the cells were captured using an inverted micro-scope (Zeiss) at 24 h and analyzed using ImageJ.

2.10. In vivo studies

2.10.1. Rat femoral model construction

The animal experiment design was approved by the Animal Care and Experiment Committee of Sun Yat-sen University (SYSU-IACUC-2023-000114). All experimental procedures and animal maintenance followed the rules of the National Institutes of Health Guide for the Care and Use of Laboratory Animals. Rat models of femoral mono-cortical defects were created as described previously and three rats were used in each group [35,36]. In brief, SD rats were injected intraperitoneally with Zoletil-50. After the animals were completely anesthetized, tweezers and hooks were used to separate the femoral surface muscles above the knee joint through an incision on the inside of the knee. After the surface of the medial tibia was clearly exposed, a spherical defect with a diameter of 1 mm was generated in the femur using a spherical drill bit and physiological saline for cooling. 5×10^4 ADSCs suspended in medium containing GelMA (Engineering for Life, China) were transferred into the osseous hole in the right femur and then immediately solidified using light. The above experiment was divided into Gel, Gel + ADSC and Gel + BPQD-modified-ADSC groups under a LPS simulated periodontitis condition. Lastly, the muscle and skin were sutured in layers. The SD rats were raised in cages and allowed free access to food and water. Finally, carbon dioxide asphyxiation was used to euthanize all rats to obtain the femur at 14 days post-operation.

2.10.2. Microcomputed tomography (micro-CT) examination

In vivo new bone formation was examined using a micro-CT device (Siemens, Munich, Germany) at 14 days. After 48 h of fixation with polyformaldehyde, the samples were scanned using a high-resolution Inveon micro-CT (Siemens) with a valid pixel size of 12.7 μm at 70 kV and 114 μA using a 1500-ms exposure time. The new bone reconstructed 3D models and bone parameter evaluation were analyzed using a professional three-dimensional analysis software (Siemens).

2.10.3. Histological evaluation

After samples were harvested on day 14, the bone was immobilized with 4 % paraformaldehyde for 2 days and then decalcified in EDTA for 30 days at room temperature. Subsequently, the decalcified bone was dehydrated in serial ethanol solutions, embedded in paraffin, and then cut into 4 μm sections. The extent of new bone formation was examined with hematoxylin and eosin (H&E, Servicebio, China) staining and Masson trichome (Servicebio) stain.

2.10.4. Immunofluorescence staining

The antigens of sections were recovered using a high pH Tris-EDTA solution. After being blocked with goat serum (Boster, China) for 30 min at room temperature, the specimens were treated with the primary antibodies Runx2 (Affinity Biosciences), OCN (Affinity Biosciences), CD68 (Elabscience, China), iNOS (Affinity Biosciences), Arg-1 (Affinity Biosciences), CD31 (Affinity Biosciences), and VEGF (Affinity Biosciences) overnight at 4 °C. This was followed by an incubation with corresponding secondary antibodies (1:400, conjugated to AlexaFluor 568 and AlexaFluor 488, Invitrogen, USA) for 1 h at room temperature. Then, the nuclei were stained with DAPI (Solarbio) for 10 min at room temperature. Finally, images of the cells were captured using a LCSM (Zeiss).

2.11. Statistical analysis

All assays were carried out at least three times. Data were analyzed using SPSS software (IBM, USA). The final results are presented as the mean ± s.d. The statistical significance was evaluated by one-way analysis of variance (ANOVA) and Student's unpaired *t*-test. A value of $^*P < 0.05$ was considered a statistically significant difference.

3. Results and discussion

3.1. Characterization of ADSCs and BPQDs

The ADSCs are long spindle shaped cells with typical fibroblast morphology (Fig. 1A), which possess osteogenic differentiation (Fig. 1B) and adipogenic differentiation abilities (Fig. 1C). Detection by flow cytometry demonstrated that the expression of ADSC surface antigen CD44 (99.98 %), and CD90 (99.97 %) were strongly positive, while the expression of CD34 (0.46 %) and CD45 (0.83 %) was negative (Fig. 1D), illustrating that the ADSCs were successfully extracted.

As demonstrated in Fig. 1E, the ultrasmall BPQDs were obtained from bulk BP powder via a liquid exfoliation method. The BPQDs obtained by centrifugation were dispersed in water and then used for ADSC culture. To investigate the characteristics of the BPQD structure, the morphology and size were measured with TEM. As demonstrated in TEM images (Fig. 1F and G), the BPQD solution is well dispersed and their morphology is close to a melon-like sphere. BPQDs have an average diameter of 7.2 ± 1.7 nm (Fig. 1H), indicating that the BPQDs were successfully synthesized. As summarized in Fig. 1I, the BPQDs possessed an electrostatic potential of −7.02 ± 1.24 mV as determined by the zeta potential in the cell culture medium (pH 7.4). The hydrodynamic size of the BPQDs in the cell culture medium (pH 7.4) was 163.53 ± 18.24 nm. Accordingly, the BPQDs had a marginally larger hydrodynamic size than the individuals examined in the TEM images, which is consistent with the characterization of BPQDs reported previously [37,38].

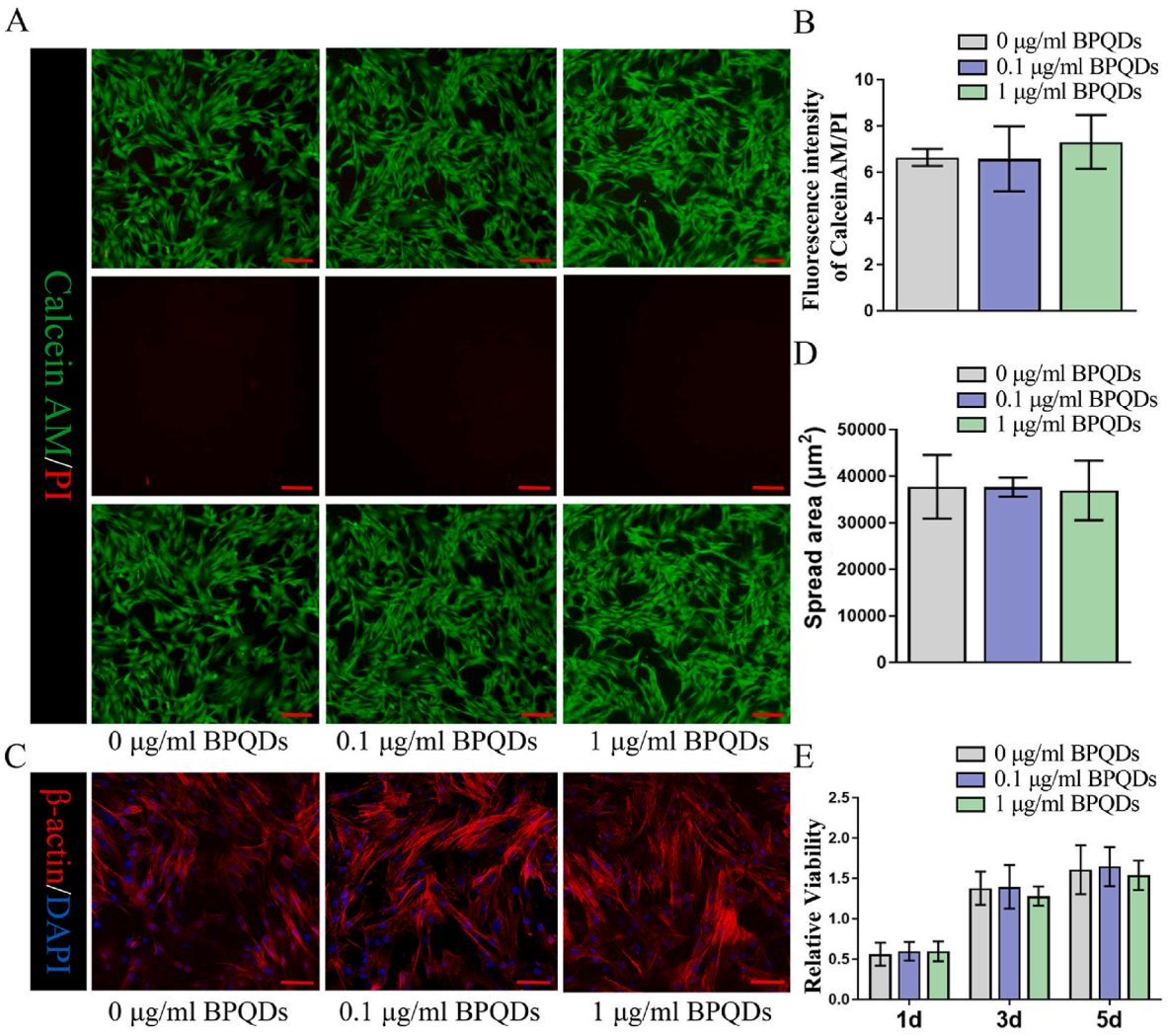

Fig. 2. In vitro biocompatibility examination of BPQDs. (A–B) Live/dead staining after 72 h and statistical analysis. Live cells are stained green and dead cells are stained red. Scale bar: 200 μm, n = 3. (C–D) Typical images of the adhesive effect and morphologic characteristics of ADSCs after 72 h of treatment with different concentrations of BPQDs. Scale bar: 100 μm, n = 3. (E) CCK8 results revealing the proliferation of ADSCs treated with different concentrations of BPQDs. Each experiment was performed in triplicate, and the data are presented as the mean ± s.d. (n = 3). The quantitative data were subjected to ANOVA for a pairwise comparison.

3.2. *In vitro biocompatibility of BPQDs*

To investigate the alveolar bone defect repair ability of BPQD-modified ADSCs, the biocompatibility of BPQDs was examined. After 72 h of culture, the ADSCs were stained with Calcein-AM/PI to evaluate the proportion of living and dead cells. No obvious cytotoxic effects were detected as a result of the BPQDs because few dead cells were observed in each sample (Fig. 2A and B). The cytoskeleton and cell nuclei of ADSCs cultured with different concentrations of BPQDs were stained with the phalloidin-TRITC and DAPI at 72 h. As shown in Fig. 2C and D, the extent of extension and adhesion quantity of the ADSCs showed no obvious differences among the samples. The proliferation of ADSCs treated with BPQDs was examined by CCK-8 assay. The results showed that the cell proliferation of ADSCs treated with BPQDs showed no significant differences at 1, 3 and 5 days (Fig. 2E).

The good biocompatibility of nanoparticles is crucial for their application in the biomedical field, and the cytotoxicity effects of nanomaterials mainly depend on factors such as the size, concentration, incubation time and type of cells [39]. According to the literature, 200 μg/ml BPQDs triggered remarkable cellular oxidative stress, apoptosis and reduced cell viability in HeLa cells [40]. In treatment of human skin fibroblast cells, human breast cancer cells and melanoma cells, BP derivatives and BPQDs (<10 nm) are supposed to be non-cytotoxic even up to a concentration of 1000 μg/ml [41]. In addition, 5–20 μg/ml BPQDs caused significant toxicity of lung cells, including a dose-dependent decrease in cell viability, lactate dehydrogenase leakage, cell morphological alteration, cellular oxidative stress and cell cycle arrest [38]. Therefore, the findings regarding BPQDs-triggered cytotoxicity have not yet reached consistent conclusions, which is likely because of the different cell types and detection indicators used. In this study, we used low concentrations of BPQDs (≤1 μg/ml) to treat ADSCs, and found that low concentrations of BPQDs showed good biocompatibility with ADSCs, which could inform further exploration.

3.3. *BPQD-modified ADSCs accelerate osteogenic effects through the Wnt/β-catenin and BMP2/SMAD5/Runx2 signaling pathways*

To explore the osteogenic ability of BPQD-modified ADSCs, ALP staining and ALP activity analyses were conducted. The levels of ALP staining of the 0.1 and 1 μg/ml BPQDs modified ADSC groups increased obviously, with more staining observed in the 1 μg/ml group (Fig. 3A). Meanwhile, the ALP activity in the 1 μg/ml group was the highest (Fig. 3B). The formation of calcified nodules of all three sample groups were examined using ARS staining and quantitative analysis, which

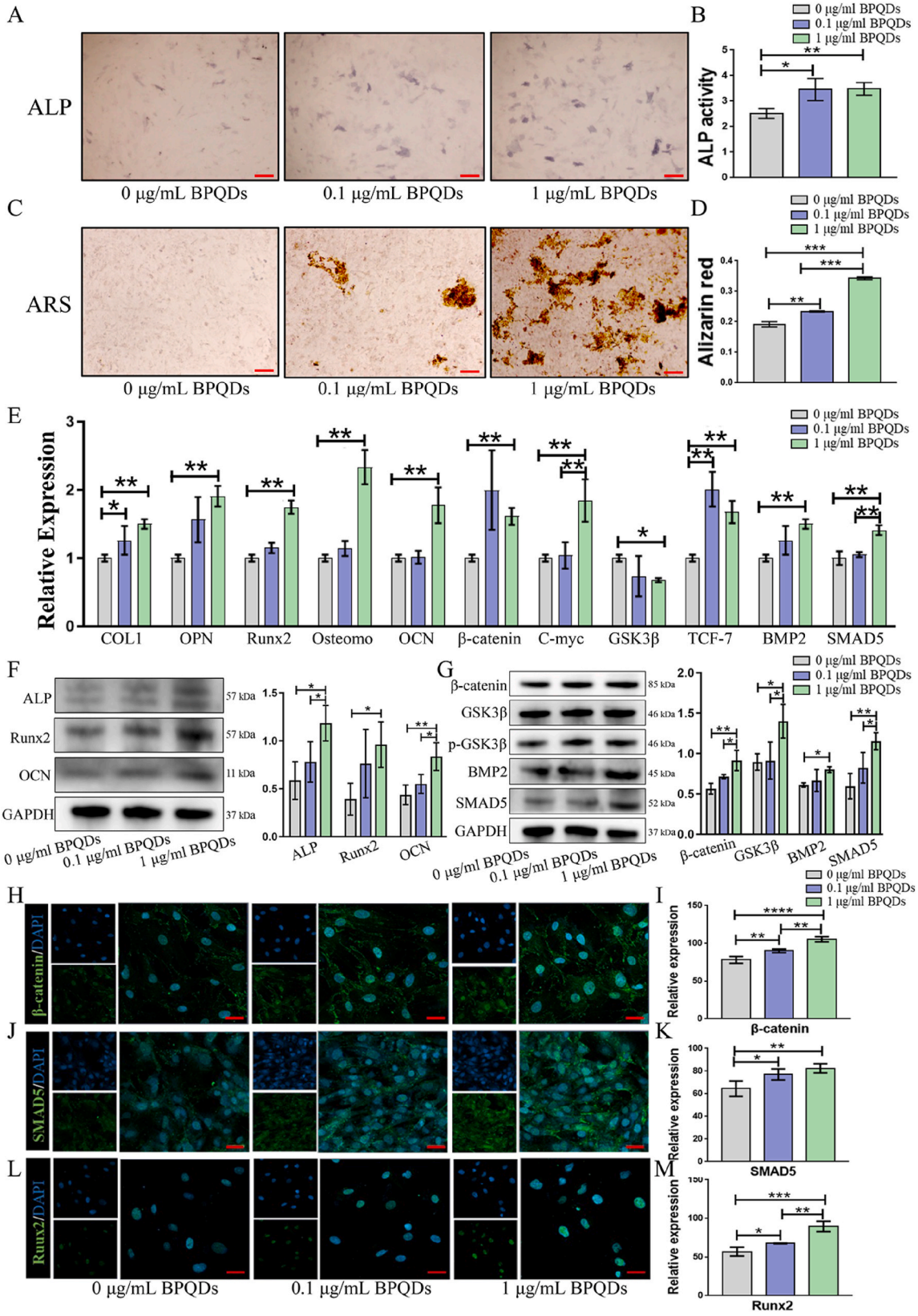

Fig. 3. BPQD-modified ADSCs accelerate osteogenic effects through the Wnt/β-catenin and BMP2/SMAD5/Runx2 signaling pathways. (A–B) ALP staining and ALP activity analysis in ADSCs cultured with BPQDs for 7d. Scale bar: 200 μm. (C–D) ARS staining and semi-quantitative examination were conducted to detect the formation of mineralized nodules in ADSCs cultured with BPQDs for 14d. Scale bar: 200 μm. (E) The mRNA expression in ADSCs cultured with BPQDs for 7d was analyzed by qPCR. (F) The osteogenic-related proteins expression in ADSCs cultured with BPQDs for 7d was detected by western blot. (G)The Wnt/β-catenin and BMP2/SMAD5/Runx2 pathway-related proteins were determined by western blot. (H–I) Cellular immunofluorescence assay showing the cellular expression of β-catenin, (J–K) SMAD5 and (L–M) Runx2 in ADSCs cultured with BPQDs for 3d. Scale bar: 50 μm. Each experiment was performed in triplicate, and the data are presented as the mean ± s.d. (n = 3). The quantitative data were subjected to ANOVA for a pairwise comparison. *$p < 0.05$, **$p < 0.01$, and ***$p < 0.001$.

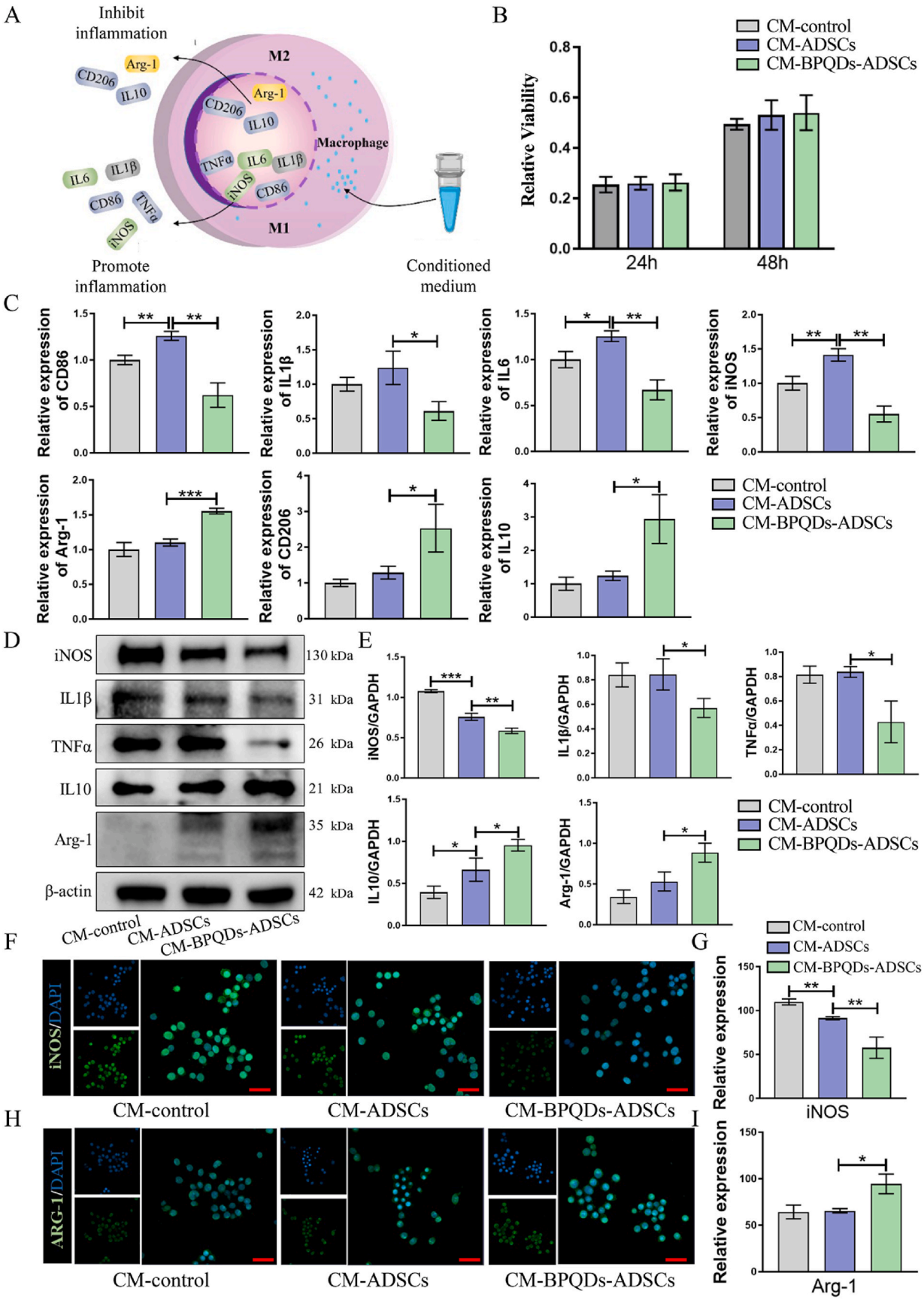

(caption on next page)

Fig. 4. Regulation of macrophage polarization after culture with BPQD-modified ADSC conditioned medium. (A) An illustration of BPQD-modified ADSC conditioned medium modulation of macrophage polarization. (B) CCK-8 was used to evaluate the proliferation of RAW 264.7 treated with complete medium, ADSC-conditioned medium and BPQD-modified ADSC conditioned medium at 24 h and 48 h. (C) qPCR was performed to detect the contents of CD86, IL1β, IL6, iNOS, Arg-1, CD206, IL10 in RAW 264.7 treated with different conditioned mediums. (D–E) Western blot assay was used to detect the expression of iNOS, IL1β, TNFα, IL10 and Arg-1 in RAW 264.7 treated with different conditioned mediums. (F–G) Immunofluorescence staining was used to examine the expression of iNOS and (H–I) the expression of Arg-1 in RAW 264.7 cultured with different conditioned mediums. iNOS or Arg-1 stained green and the nuclei stained blue. Scale bar: 40 μm. Each experiment was performed in triplicate, and the data are presented as the mean ± s.d. (n = 3). The quantitative data were subjected to Student's t-test for a pairwise comparison. *p < 0.05, **p < 0.01, and ***p < 0.001.

showed that the 1 μg/ml BPQD-modified ADSC group was the most apparent, exhibiting a dark red color (Fig. 3C and D). ALP is an important marker of early osteogenic differentiation. Meanwhile, the matrix mineralization is an important marker of late osteogenic differentiation [42]. Additionally, the expression of five osteogenic genes (COL1, OPN, Runx2, osteomodulin and OCN) in ADSCs cultured for 7 days was examined by qPCR, as shown in Fig. 3E. The expression trend showed that using 1 μg/ml BPQDs to modify ADSCs could significantly promote these five osteogenic genes, while this effect was not obvious with 0.1 μg/ml BPQDs. Western blot assay was to examine the protein expression of ALP, Runx2 and OCN in ADSCs treated for 7 days, as shown in Fig. 3F. The gray scale of protein bands in the 1 μg/ml BPQD-modified ADSC group significantly increased, demonstrating that the protein expression was in accord with the gene expression. These results demonstrated that BPQDs could modify ADSCs to accelerate the osteogenic effect, which exhibited a concentration-dependent manner. Compared with 0.1 μg/ml, the use of 1 μg/ml BPQDs to modify ADSCs showed a stronger osteogenic-inducing effect.

Wnt/β-catenin [43] and BMP2/SMAD5/Runx2 [44] are important signaling pathways for osteogenic effects. Wnt/β-catenin pathway activation relies on cell membrane binding of Wnt and LRP co-receptor and frizzled receptor, which decreases the glycogen synthase kinase-3β (GSK3β) level and stabilizes β-catenin in the cytosol, increasing its nucleus translocation. Furthermore, β-catenin promotes transcription regulated by T-cell factor 4 (TCF4)/lymphoid enhancing factor-1 (LEF1), thereby initiating the transcription of downstream target genes such as Runx2, and ultimately promoting osteogenic differentiation [43]. SMADs are signal sensors of TGF-β superfamily members, among which SMAD5 can promote BMP2 signal transduction and start the transcription of downstream target genes, thereby promoting osteogenic effects [44]. qPCR was used to detect the expression of genes (β-catenin, C-myc, CSK3β, TCF-7, BMP2 and SMAD5) in ADSCs cultured for 7 days, as shown in Fig. 3E. The expression trend showed that the use of 1 μg/ml BPQDs to modify ADSCs significantly promoted β-catenin, C-myc, TCF-7, BMP2 and SMAD5 and decreased CSK3β. Western blot analysis further demonstrated that the use of 1 μg/ml BPQDs to modify ADSCs significantly promoted β-catenin, pGSK3β, BMP2 and SMAD5 expression compared with the control group (Fig. 3G). The immunofluorescence staining results demonstrated that the use of 0.1 μg/ml or 1 μg/ml BPQDs to modify ADSCs significantly upregulated β-catenin expression (Fig. 3H and I), SMAD5 expression (Fig. 3J and K) and Runx2 expression (Fig. 3L, M) when compared to the control group, which was more obvious in the 1 μg/ml BPQD-modified ADSC group. These results indicated that using BPQDs to modify ADSCs could accelerate the osteogenic effect without adding osteogenic induction medium via the Wnt/β-catenin and BMP2/SMAD5/Runx2 signaling pathway.

3.4. Regulation of macrophage polarization cultured with BPQD-modified ADSC conditioned medium

As shown in Fig. 4A, the activated M1 phenotype can secrete a great quantities of pro-inflammatory cytokines, including IL1β, IL6, tumor necrosis factor alpha (TNFα) and inducible nitric oxide synthase (iNOS), which can cause chronic inflammation and impede bone regeneration [45]. An activated M2 phenotype can promote the osteogenic capacity by producing a great quantity of anti-inflammatory cytokines, like IL10 and arginine 1 (Arg-1), which usually activate cell proliferation, extracellular matrix synthesis and bone tissue remodeling in the latter phase [45]. Evidence suggests that the therapeutic effect of mesenchymal stem cells (MSCs) is largely facilitated by paracrine mechanisms to excite the activity of tissue-resident cells. During bone regeneration, macrophage/MSCs crosstalk is crucial for bone regeneration [46]. Aberrant immunomodulation (enhancement or suppression) may inhibit bone regeneration via blocking the transformation of macrophages from the M1 to M2 phenotype [47,48]. Furthermore, we treated the macrophage cell line RAW 264.7 with BPQD-modified ADSC CMs to investigate the effects of the polarization of macrophages via paracrine pathway. As shown in Fig. 4B,CCK-8 was used to evaluate the proliferation of RAW 264.7 treated with CMs. The results showed that cell viability of RAW 264.7 treated with CM-ADSCs and CM-BPQDs-ADSCs was slightly increased at 48 h but not statistically different from the control group. RAW 264.7 were cultured under inflammatory conditions with different concentrations of LPS determined by qPCR before each experiment. The results showed that 50 ng/ml LPS could increase the M1 marker expression of CD86, IL1β and iNOS and decrease the M2 marker expression of CD206 and Arg-1 in RAW 264.7 (Fig S1).

The gene expression level, immunofluorescence staining and western blot assays were applied to examine the inflammation regulatory effect of each group of RAW 264.7 treated with the CMs under an inflammation microenvironment simulated by 50 ng/ml LPS for 2 days. The qPCR results showed that the CD206, Arg-1 and IL10 expression were higher while the CD86, IL6 and iNOS expression were lower in the CM-BPQDs-ADSC group than in the CM-ADSC group (Fig. 4C), which indicated that BPQD-modified ADSCs could secrete some factors to induce beneficial immune response in the host by transferring a majority of macrophage polarization from the M1 to the M2 phenotype. Nevertheless, the comparison between the CM-ADSC and CM-control groups revealed no significant difference. Western blot analysis further confirmed that CM-BPQDs-ADSCs significantly inhibited the expression of iNOS, IL1β and TNFα, yet promoted the expression of Arg-1 and IL10 in RAW 264.7 compared with the other groups under the LPS culture condition (Fig. 4D and E). Meanwhile, RAW 264.7 in the CM-BPQDs-ADSC group featured a lower percentage of iNOS-positive cells (Fig. 4F, G) and a higher percentage of Arg-1-positive cells compared with the other groups (Fig. 5H and I) under the inflammatory culture condition. It is well known that macrophages are highly plastic, mainly displaying pro-inflammatory (M1) which can cause chronic inflammation to decrease bone regeneration and anti-inflammatory (M2) phenotypes, which usually activate cell proliferation, extracellular matrix synthesis and tissue remodeling in the latter phase [49]. Avoiding an excessive inflammatory response to promote M1-to-M2 polarization is critical for angiogenesis and bone regeneration [50,51]. All of the above results suggested that BPQD-modified ADSCs could propel the conversion of M1 macrophages to M2 via a paracrine pathway, which might provide theoretical support for further elucidating the improvement of alveolar bone defect repair in an LPS simulated periodontitis microenvironment.

3.5. Effects on cellular behaviors and osteogenic effect of BMSCs cultured with BPQD-modified ADSC conditioned medium in the periodontitis microenvironment

BMSCs exist in bone marrow, and are prevalent stem cells in the field of tissue engineering and regenerative medicine [52]. When bone defects occur, osteoblasts reduce quickly, impeding the potential of bone

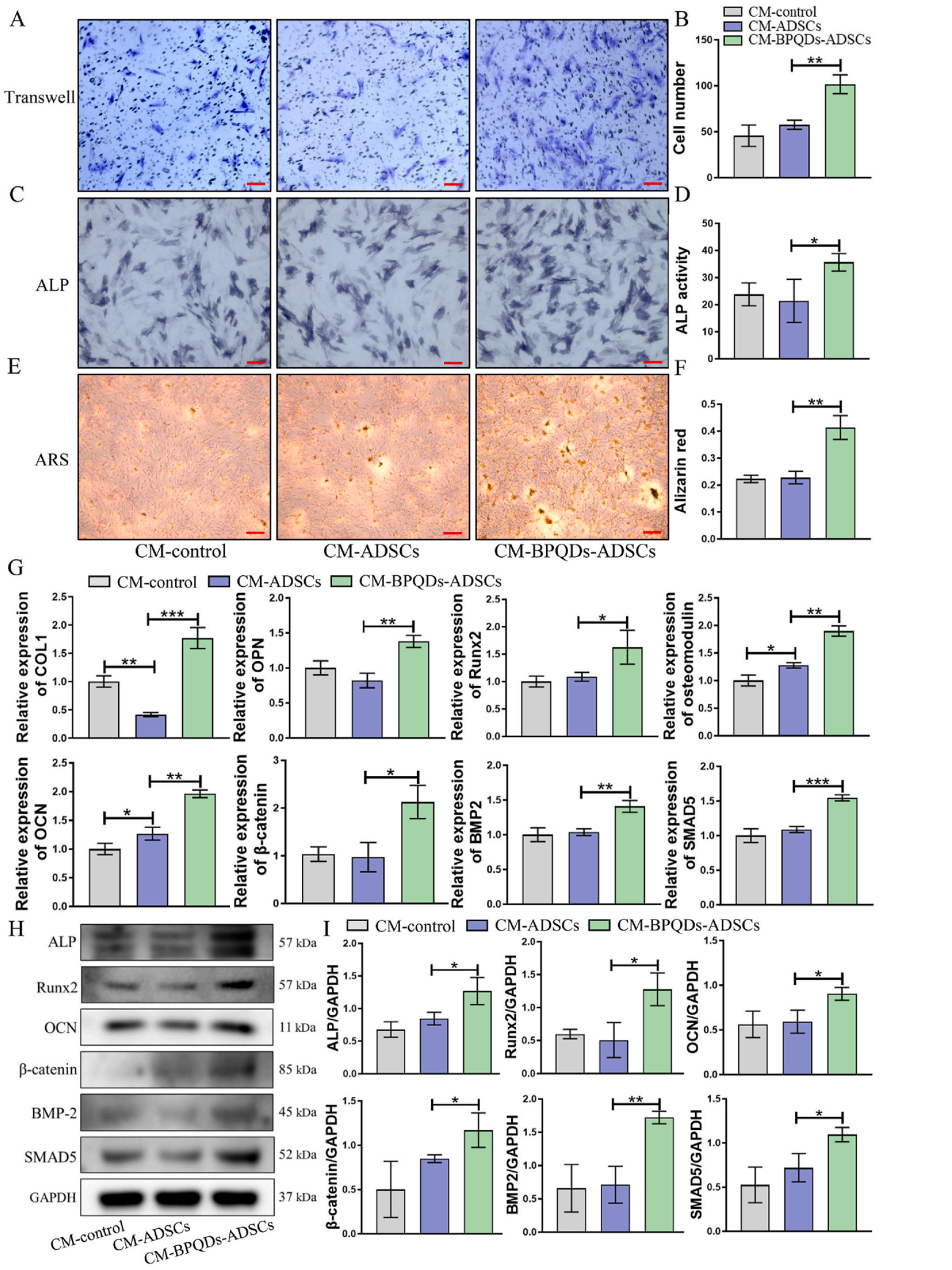

(caption on next page)

Fig. 5. Effects on cellular behaviors and the osteogenic effect of BMSCs cultured with BPQD-modified ADSC conditioned medium in the periodontitis microenvironment. (A–B) Transwell assays were used to detect the migration ability of BMSCs, and photographs were taken 24 h after treatment with complete medium, ADSC-conditioned medium or BPQD-modified ADSC conditioned medium under the LPS condition. Scale bar: 100 μm. (C–D) The ALP staining and ALP activity was determined in BMSCs after the addition of complete medium, ADSC-conditioned medium or BPQD-modified ADSC conditioned medium under the LPS condition. Scale bar: 200 μm. (E–F) ARS staining and semi-quantitative analysis to examine the mineralized nodule formation after treatment with different conditioned mediums under the LPS condition. Scale bar: 200 μm. (G) The osteogenic-related mRNA expression in BMSCs was examined by qPCR. (H–I) Detection of osteogenic-related proteins in BMSCs by western blot under the LPS condition. Each experiment was performed in triplicate, and the data are presented as the mean ± s.d. (n = 3). The quantitative data were subjected to Student's t-test for a pairwise comparison. *$p < 0.05$, **$p < 0.01$, and ***$p < 0.001$.

damage recovery in the deficient area. Activating tissue-resident BMSCs activity can expand the number of osteoblasts and thus improve bone regeneration [53,54]. To evaluate the effect of paracrine function of BPQD-modified ADSCs on cell behaviors and osteogenic effects in the periodontitis microenvironment, the BMSCs were treated with condition mediums (CMs) extracted from ADSCs cultured with 50 ng/ml LPS. The results showed that the BMSCs have a long spindle shape (Fig. S2A), which possess osteogenic differentiation (Fig. S2B) and adipogenic differentiation abilities (Fig. S2C). Examination by flow cytometry showed that the expression of BMSC surface antigens CD44 (99.98 %), and CD90 (99.95 %) were strongly positive, while the expression of CD34 (1.14 %) and CD45 (1.96 %) was negative (Fig. S2D), illustrating that the BMSCs were successfully isolated. The cell behaviors of BMSCs treated with different CMs was detected by CCK-8 and transwell assays in a LPS simulated inflammatory microenvironment. The CCK8 result showed that cell proliferation of BMSCs treated with CM-ADSCs and CM-BPQDs-ADSCs was slightly decreased after 1, 3 and 5 days, but not statistically different from the control group (Fig. S3). The transwell assay revealed that the CM-BPQDs-ADSCs significantly increased the migration ability of BMSCs compared to the CM-ADSCs and control (Fig. 5A and B), which indicated that BPQD-modified ADSCs could promote the migration ability of BMSCs through paracrine pathways, which might be beneficial for the BMSCs to home in on the inflammatory bone defect region.

The osteogenic effect of the BMSCs was evaluated using ALP staining and ARS under the LPS condition after 7 days of co-culture. As shown in Fig. 5C and D, the secretion from BPQD-modified ADSCs significantly promoted the ALP expression and activity in BMSCs when compared with the control and CM-ADSC groups. The mineralized nodule formation of BMSCs was visibly increased in the CM-BPQDs-ADSCs, as shown by ARS staining comparison with the control and CM-ADSC groups (Fig. 5E and F), which resembles the ALP staining and ALP activity evaluation tendency. Previous studies have shown that the activation of Wnt/β-catenin and BMP2/SMAD5/Runx2 signaling pathways plays important roles in osteogenesis under an inflammation microenvironment [23,55]. Under the condition of a LPS simulated periodontitis microenvironment, BMSCs co-cultured with CM-BPQDs-ADSCs showed higher gene expression, including COLI, OPN, Runx2, osteomodulin, OCN, β-catenin, BMP2, and SMAD5 (Fig. 5G), and higher protein expression, including ALP, Runx2, OCN, β-catenin, BMP2 and SMAD5 when compared with other groups (Fig. 5H and I). The above outcomes revealed that BPQD-modified ADSCs could promote the osteogenic effect of BMSCs through a paracrine pathway in a periodontitis microenvironment, which is associated with Wnt/β-catenin and BMP2/SMAD5/Runx2 signaling pathway regulation. Therefore, we speculated that enhancing the homing and osteogenic ability of BMSCs in the local inflammatory bone defect region might be another important beneficial factor for the use of BPQD-modified ADSCs to improve the efficacy of alveolar bone repair in periodontitis.

3.6. Angiogenesis induced by BPQD-modified ADSC conditioned medium in the periodontitis microenvironment

In the process of bone regeneration, angiogenesis and osteogenesis process are closely connected [56]. The blood vessels can support more indispensable oxygen, metabolites, and nutrients, and it has been reported that vascularization plays an important role in bone defect repair [57]. To evaluate the effects of BPQD-modified ADSCs on angiogenesis in the periodontitis microenvironment, we used an indirect co-culture model to examine the angiogenesis ability of HUVECs via scratch test, CCK8 assay, transwell assay, and tube formation experiments under the condition of 50 ng/ml LPS. After being cultured with different CMs, the horizontal migration ability of HUVECs showed no statistical differences among the CM-BPQDs-ADSC, CM-ADSC and CM-Control groups in the scratch experiment evaluation (Fig. 6A and B). The CCK8 assays results showed that HUVECs treated with CM-ADSCs and CM-BPQDs-ADSCs were slightly increased at 24 and 48 h compared with the control group, but there was no statistical difference among them (Fig. 6C). In addition, the horizontal migration ability was examined via transwell experiment. After HUVECs were cultured with different CMs, the results exhibited no statistical differences among the CM-BPQDs-ADSC, CM-ADSC and CM-Control groups (Fig. 6D and E). Furthermore, tube formation experiments showed that CM-BPQDs-ADSCs slightly enhanced the angiogenesis of HUVECs compared with the other groups, however, there was no statistical significance (Fig. 6F and G). In addition, the qPCR results showed that there were no significant changes in angiogenic genes including CD31, VEGF and ANG1 in HUVECs among the CM-BPQDs-ADSC, CM-ADSC and CM-Control groups (Fig. 6H). Altogether, the results suggested that BPQD-modified ADSCs did not promote angiogenesis of endothelial cells in the periodontitis microenvironment through paracrine pathways.

3.7. Results of in vivo bone defect repair in the periodontitis microenvironment

Two weeks after the operation, a micro-CT, which can provide reconstructed 3D images and quantitative analyses data of newly regeneration bone, was used to examine the extracted femur bone specimens. As the 3D reconstructed images of the samples showed, the extent of growth of newborn bone in the BPQD-modified ADSC group was significantly higher than that the other groups (Fig. 7A). The quantitative analyses of the new bone formation region, including the BV/TV and BMD are displayed in Fig. 7B and C. The BV/TV and BMD were the highest in the BPQD-modified ADSC group, and there was no statistical difference between the ADSC group and the control group. Additionally, to further identify the osteogenesis occurring in vivo, the bone defect area was stained with H&E and Masson's trichrome. At 2 weeks, the H&E staining results revealed that a large amount of bone tissue had formed in the BPQD-modified ADSC group, with a denser bony structure than observed in the other groups (Fig. 7D). Masson's trichrome staining showed that the BPQD-modified ADSC group possessed a significantly more collagen fiber formation than other groups after 2 weeks (Fig. 7E and F). Furthermore, the immunofluorescence staining results revealed that the expression of osteogenic markers including Runx2 (Fig. 7G and H) and OCN expression (Fig. 7I and J) in the bone tissue was the strongest in the BPQD-modified ADSC group.

To further evaluate the osteoimmunomodulatory properties in the bone defect region, immunofluorescence staining was used to examine the polarization status of macrophages. CD68 is a pan marker for in situ macrophages [58]. $CD68^{+}$ cells were observed in samples from all groups, demonstrating that macrophages were effective in the response to the bone healing process in the bone defect [59]. Immunofluorescence staining for M2 (Arg-1) and M1 (iNOS) markers was used to assess

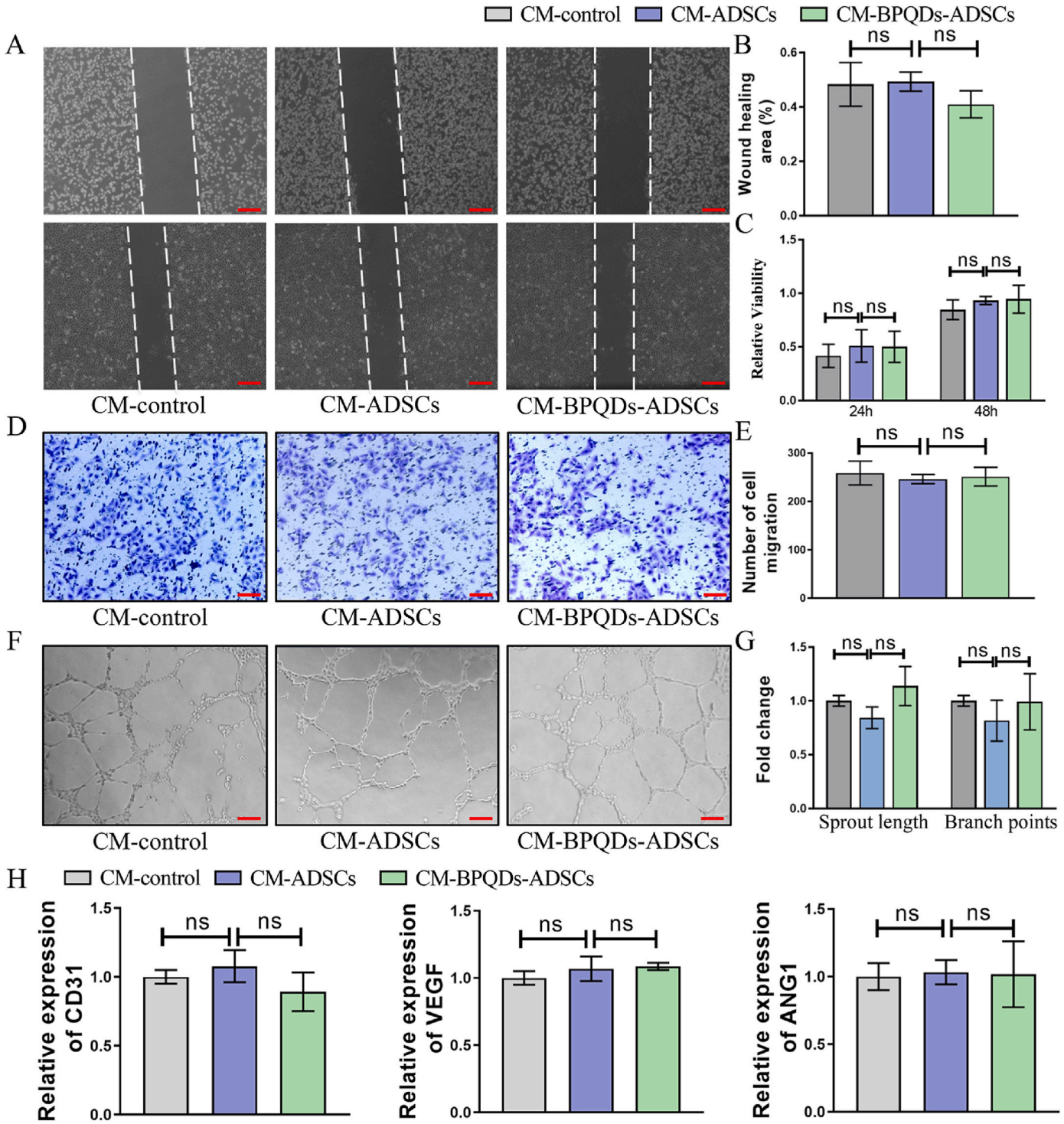

Fig. 6. The angiogenesis induced by BPQD-modified ADSC conditioned medium in the periodontitis microenvironment. (A–B) A scratch assay was used to detect the migration ability of HUVECs, and photographs were taken 0 and 24 h after adding complete medium, ADSC-conditioned medium or BPQD-modified ADSC conditioned medium under the LPS condition. Scale bar: 200 μm. (C) CCK8 results revealed the proliferation of HUVECs treated with complete medium, ADSC-conditioned medium and BPQD-modified ADSC conditioned medium under the LPS condition at 24 h and 48 h. (D–E) Transwell assays were conducted to detect the migration ability of HUVECs under the LPS condition, and photographs were taken at 24 h. Scale bar: 100 μm. (F–G) Tube formation analysis of the angiogenesis of HUVECs treated with complete medium, ADSC-conditioned medium and BPQD-modified ADSC conditioned medium at 24 h under the LPS condition. Scale bar: 100 μm. (H) qPCR analysis of the gene expression of CD31, VEGF, and ANG1 in the HUVECs under the LPS condition. Each experiment was performed in triplicate, and the data are presented as the mean ± s.d. (n = 3). The quantitative data were subjected to Student's t-test for a pairwise comparison. ns represents no significance.

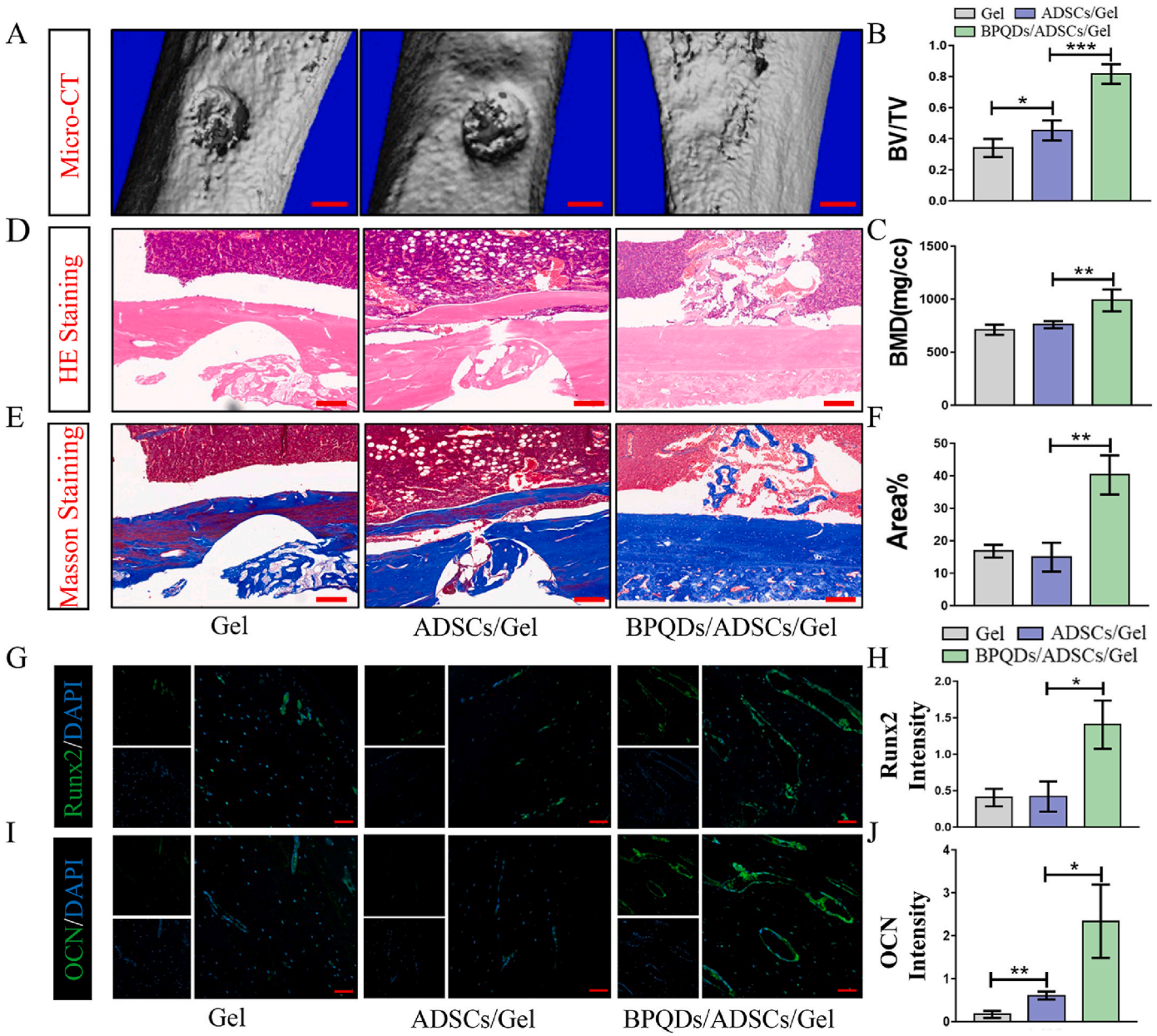

Fig. 7. Results of in vivo bone defect repair in the periodontitis microenvironment. (A) Typical micro-CT images revealed new bone formation ability in a femoral mono-cortical defect model after being treated with gel alone, ADSCs/gel or BPQD-modified-ADSCs/gel. Scale bar: 500 μm. (B–C) Micro-CT quantitative results demonstrating the BV/TV and BMD. (D) H&E staining was used to examine the new bone regeneration. Scale bar: 200 μm. (E–F) Masson's trichrome staining for detection of collagen formation in the new bone regeneration region. Triangle: native bone; Star: new bone. Scale bar: 200 μm. (G–H) Representative immunofluorescence staining images of the expression of Runx2 and (I–J) The expression of OCN in the bone regeneration area. Scale bar: 50 μm. Each group contained three rats (n = 3), and the data are presented as the mean ± s.d. The quantitative data were subjected to Student's t-test for a pairwise comparison. *$p < 0.05$, **$p < 0.01$, and ***$p < 0.001$.

the macrophage phenotype. More Arg-1$^+$ (Fig. 8A and B) and fewer iNOS$^+$ cells (Fig. 8C and D) were stained in the BPQD-modified ADSC group than the other groups, revealing that transplantation of BPQD-modified ADSCs could transform macrophages from the M1 phenotype to the M2 phenotype in the inflammation bone defect model. Nevertheless, no remarkable difference was detected between the ADSC group and the control group. Interestingly, in the bone and the surrounding fibroblastic-like tissue, the expression of angiogenic markers including CD31 (Fig. 8E and F) and VEGF (Fig. 8G and H) in the BPQD-modified ADSC group was also observed to be the most obvious among all the groups, however, in the pure ADSC group, no obvious positive staining was detected at 2 weeks' post-transplantation. During bone defect repair, the formation of blood vessels is closely related with bone regeneration, and blood vessel formation is a prerequisite for bone regeneration. In bone tissue, rapid vascularization can support sufficient nutrition for the function and activity of osteoblasts and determine the quantity of new bone growth [57]. The results (Fig. 6) showed that BPQD-modified ADSCs did not promote proliferation, migration and angiogenesis in HUVECs through paracrine pathways. Macrophages tend to polarize towards the M1 phenotype in the inflammation phase, and increase the secretion of pro-inflammatory cytokines such as TNFα, IL1β, and iNOS, which can exacerbate harmful inflammatory responses [51,60]. However, in the repair phase, macrophages of the M2 phenotype generally prerequisite high expression of IL10, Arg-1, BMP2, and VEGF factors, which suppress inflammation, recruit osteoprogenitor cells, and activate angiogenesis, tissue remodeling, and bone

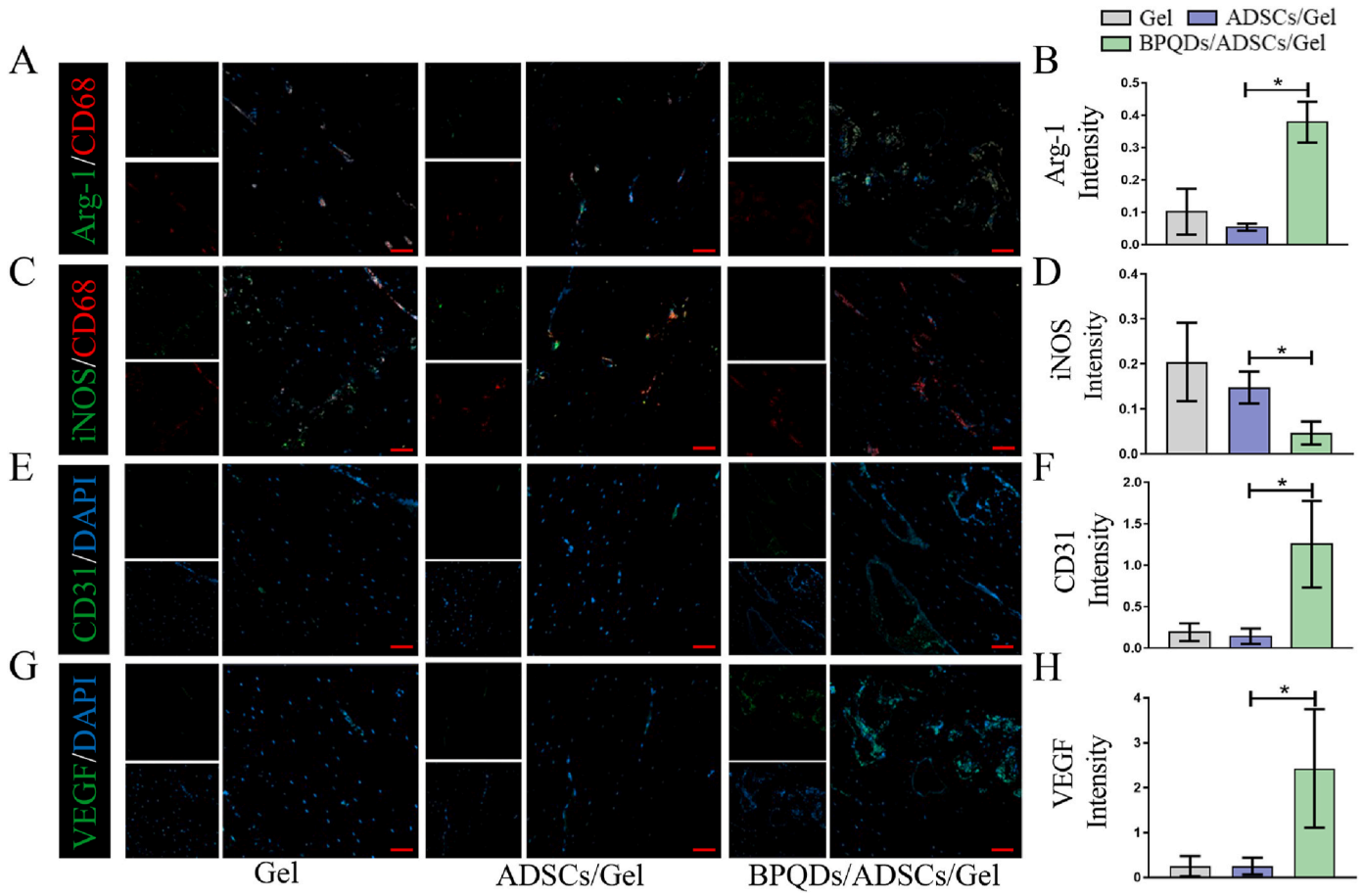

Fig. 8. Osteoimmunomodulation and angiogenesis effects in the in vivo periodontitis microenvironment. (A–B) Immunofluorescence staining was used to examine the macrophage polarization markers including Arg-1 and (C–D) iNOS in the bone defect repair region. Scale bar: 50 μm. (E–F) Immunofluorescence staining was applied to detect the angiogenic markers including CD31 and (G–H) VEGF in the bone defect repair region. Scale bar: 50 μm. Each group contained three rats (n = 3), and the data are presented as the mean ± s.d. The quantitative data were subjected to Student's t-test for a pairwise comparison. *p < 0.05.

regeneration [61–63]. Therefore, we speculated that the reason for vascularization capacity enhancement can be attributed to BPQD-modified ADSCs polarization of a great number of macrophages from the M1 phenotype to M2 in the periodontitis microenvironment.

4. Conclusion

In summary, the effects of BPQD-modified ADSCs in bone defect repair under the periodontitis microenvironment were investigated and the underlying mechanisms were examined. This study indicated that BPQDs showed good biocompatibility with ADSCs and BPQD-modified ADSCs could accelerate bone regeneration in a periodontitis microenvironment in vivo by promoting osteogenic differentiation and regulating the balance of osteoimmunomodulation. The mechanism of BPQD-modified ADSCs acceleration of osteogenic ability is through the Wnt/β-catenin and BMP2/SMAD5/Runx2 signaling pathways. Moreover, BPQD-modified ADSCs accelerated migration and osteogenic differentiation of BMSCs and facilitated the polarization of macrophages from the M1 phenotype towards the M2 phenotype transformation through the paracrine pathway in the periodontitis microenvironment. Overall, we demonstrated that BPQD-modified ADSCs could boost the repair efficiency of bone defects in the periodontitis microenvironment by modulating the cross-talk between osteogenesis and osteoimmunemodulation via endogenous osteogenic differentiation and exogenous paracrine pathways, which provides a novel and promising feasible strategy for the repair of alveolar bone defects in periodontitis.

CRediT authorship contribution statement

Yi He: Writing – original draft, Conceptualization. **Yuquan Tang:** Investigation, Conceptualization. **Binghui Zeng:** Investigation. **Xun Chen:** Formal analysis. **Linyu Yuan:** Formal analysis. **Yunyang Lu:** Investigation. **Weidong Du:** Methodology. **Runze Li:** Software. **Yaolin Han:** Formal analysis. **Feilong Deng:** Writing – review & editing. **Dongsheng Yu:** Project administration, Funding acquisition. **Wei Zhao:** Project administration, Funding acquisition.

Declaration of competing interest

The authors declare that they have no known competing financial interests or personal relationships that could have appeared to influence the work reported in this paper.

Data availability

Data will be made available on request.

Acknowledgements

This study was supported by the National Natural Science Foundation of China (No. 82073378, 82373255 and 81974146), the Guangdong Science and Technology Project (2021A1515012399 and 2023A1515012554), and the Special Fund Project for Science and Technology Innovation Strategy of Guangdong Province

(pdjh2024b017).

Appendix A. Supplementary data

Supplementary data to this article can be found online at https://doi.org/10.1016/j.mtbio.2024.101122.

References

[1] K. Jepsen, A. Sculean, S. Jepsen, Complications and treatment errors involving periodontal tissues related to orthodontic therapy, Periodontol. 2000 92 (1) (2023) 135–158.
[2] D.F. Kinane, P.G. Stathopoulou, P.N. Papapanou, Periodontal diseases, Nat. Rev. Dis. Prim. 3 (2017) 17038.
[3] A.D. Lietzan, J.B. Simpson, W.G. Walton, P.B. Jariwala, Y. Xu, M.H. Boynton, J. Liu, M.R. Redinbo, Microbial β-glucuronidases drive human periodontal disease etiology, Sci. Adv. 9 (18) (2023) eadg3390.
[4] R. Kobayashi, T. Hashizume-Takizawa, T. Kurita-Ochiai, Lactic acid bacteria prevent both periodontitis and atherosclerosis exacerbated by periodontitis in spontaneously hyperlipidemic mice, J. Periodontal. Res. 56 (4) (2021) 753–760.
[5] T. Ding, W. Kang, J. Li, L. Yu, S. Ge, An in situ tissue engineering scaffold with growth factors combining angiogenesis and osteoimmunomodulatory functions for advanced periodontal bone regeneration, J. Nanobiotechnol. 19 (1) (2021) 247.
[6] Y. He, G. Chen, Y. Li, Y. Li, C. Yi, X. Zhang, H. Li, B. Zeng, C. Wang, W. Xie, W. Zhao, D. Yu, Effect of magnetic graphene oxide on cellular behaviors and osteogenesis under a moderate static magnetic field, Nanomedicine 37 (2021) 102435.
[7] F.I. Alagboso, G.K. Mannala, N. Walter, D. Docheva, C. Brochhausen, V. Alt, M. Rupp, Rifampicin restores extracellular organic matrix formation and mineralization of osteoblasts after intracellular Staphylococcus aureus infection, Bone Joint Res 11 (5) (2022) 327–341.
[8] Q. Zhang, M. Xin, S. Yang, Q. Wu, X. Xiang, T. Wang, W. Zhong, M.N. Helder, R. T. Jaspers, J.L. Pathak, Y. Xiao, Silica nanocarrier-mediated intracellular delivery of rapamycin promotes autophagy-mediated M2 macrophage polarization to regulate bone regeneration, Mater Today Bio 20 (2023) 100623.
[9] Y. Zhang, J. Wei, X. Yu, L. Chen, R. Ren, Y. Dong, S. Wang, M. Zhu, N. Ming, Z. Zhu, C. Gao, W. Xiong, CXCL chemokines-mediated communication between macrophages and BMSCs on titanium surface promotes osteogenesis via the actin cytoskeleton pathway, Mater Today Bio 23 (2023) 100816.
[10] Y. Zhang, J. Cao, M. Jian, Z. Zhou, N. Anwar, L. Xiao, Y. Ma, D. Zhang, J. Zhang, X. Wang, Fabrication of interleukin-4 encapsulated bioactive microdroplets for regulating inflammation and promoting osteogenesis, Int. J. Nanomed. 18 (2023) 2019–2035.
[11] R. Hang, Z. Wang, H. Wang, Y. Zhang, Y. Zhao, L. Bai, X. Yao, Matrix stiffness-induced platelet activation determines immunomodulation of macrophages, Biomater. Adv. 148 (2023) 213356.
[12] D. Wang, Y. Liu, S. Diao, L. Shan, J. Zhou, Long non-coding RNAs within macrophage-derived exosomes promote BMSC osteogenesis in a bone fracture rat model, Int. J. Nanomed. 18 (2023) 1063–1083.
[13] T.A. Wynn, K.M. Vannella, Macrophages in tissue repair, regeneration, and fibrosis, Immunity 44 (3) (2016) 450–462.
[14] B. Wu, Y. Tang, K. Wang, X. Zhou, L. Xiang, Nanostructured titanium implant surface facilitating osseointegration from protein adsorption to osteogenesis: the example of TiO(2) NTAs, Int. J. Nanomed. 17 (2022) 1865–1879.
[15] M.G. Burger, A. Grosso, P.S. Briquez, G.M.E. Born, A. Lunger, F. Schrenk, A. Todorov, V. Sacchi, J.A. Hubbell, D.J. Schaefer, A. Banfi, N. Di Maggio, Robust coupling of angiogenesis and osteogenesis by VEGF-decorated matrices for bone regeneration, Acta Biomater. 149 (2022) 111–125.
[16] U. Saran, S. Gemini Piperni, S. Chatterjee, Role of angiogenesis in bone repair, Arch. Biochem. Biophys. 561 (2014) 109–117.
[17] X. Fu, P. Liu, D. Zhao, B. Yuan, Z. Xiao, Y. Zhou, X. Yang, X. Zhu, C. Tu, X. Zhang, Effects of nanotopography regulation and silicon doping on angiogenic and osteogenic activities of hydroxyapatite coating on titanium implant, Int. J. Nanomed. 15 (2020) 4171–4189.
[18] I. Ullah, R.B. Subbarao, G.J. Rho, Human mesenchymal stem cells - current trends and future prospective, Biosci. Rep. 35 (2) (2015).
[19] L. Mazini, L. Rochette, B. Admou, S. Amal, G. Malka, Hopes and limits of adipose-derived stem cells (ADSCs) and mesenchymal stem cells (MSCs) in wound healing, Int. J. Mol. Sci. 21 (4) (2020).
[20] G. Storti, M.G. Scioli, B.S. Kim, A. Orlandi, V. Cervelli, Adipose-derived stem cells in bone tissue engineering: useful tools with new applications, Stem Cell. Int. 2019 (2019) 3673857.
[21] M. Madrigal, K.S. Rao, N.H. Riordan, A review of therapeutic effects of mesenchymal stem cell secretions and induction of secretory modification by different culture methods, J. Transl. Med. 12 (2014) 260.
[22] S.H. Bhang, S. Lee, J.Y. Shin, T.J. Lee, H.K. Jang, B.S. Kim, Efficacious and clinically relevant conditioned medium of human adipose-derived stem cells for therapeutic angiogenesis, Mol. Ther. : the journal of the American Society of Gene Therapy 22 (4) (2014) 862–872.
[23] S. Li, J. Sun, J. Yang, Y. Yang, H. Ding, B. Yu, K. Ma, M. Chen, Gelatin methacryloyl (GelMA) loaded with concentrated hypoxic pretreated adipose-derived mesenchymal stem cells(ADSCs) conditioned medium promotes wound healing and vascular regeneration in aged skin, Biomater. Res. 27 (1) (2023) 11.
[24] R.Y. Ren, J.C. Guo, H. Song, Y. Wei, C. Luo, Y.Y. Zhang, L.X. Chen, B. Gao, J.J. Fu, W. Xiong, A novel implant surface modification mode of Fe3O4-containing TiO2 nanorods with sinusoidal electromagnetic field for osteoblastogenesis and angiogenesis, Materials Today Bio 19 (2023).
[25] G. Chen, S.H. Deng, M.X. Zuo, J. Wang, D. Cheng, B. Chen, Non-viral CRISPR activation system targeting VEGF-A and TGF-81 for enhanced osteogenesis of pre-osteoblasts implanted with dual-crosslinked hydrogel, Materials Today Bio 16 (2022).
[26] S. Anju, J. Ashtami, P.V. Mohanan, Black phosphorus, a prospective graphene substitute for biomedical applications, Mater. Sci. Eng., C 97 (2019) 978–993.
[27] X. Liu, A.L. Miller 2nd, S. Park, M.N. George, B.E. Waletzki, H. Xu, A. Terzic, L. Lu, Two-dimensional black phosphorus and graphene oxide nanosheets synergistically enhance cell proliferation and osteogenesis on 3D printed scaffolds, ACS Appl. Mater. Interfaces 11 (26) (2019) 23558–23572.
[28] Y. Xiong, C. He, X. Lin, K. Cheng, F.M. He, J.X. Zhao, M.J. Yang, H. Gao, F.J. He, X. P. Zhang, Z.Q. Liu, G. Liu, W.B. Deng, Black phosphorus nanosheets inhibit glioblastoma cell migration and invasion through modulation of WNT/β-catenin and NOTCH signaling pathways, Chem. Eng. J. 481 (2024).
[29] X. Zhang, H. Xie, Z. Liu, C. Tan, Z. Luo, H. Li, J. Lin, L. Sun, W. Chen, Z. Xu, L. Xie, W. Huang, H. Zhang, Black phosphorus quantum dots, Angew Chem. Int. Ed. Engl. 54 (12) (2015) 3653–3657.
[30] S.N. Baker, G.A. Baker, Luminescent carbon nanodots: emergent nanolights, Angew Chem. Int. Ed. Engl. 49 (38) (2010) 6726–6744.
[31] X. Zhang, Z. Zhang, S. Zhang, D. Li, W. Ma, C. Ma, F. Wu, Q. Zhao, Q. Yan, B. Xing, Size effect on the cytotoxicity of layered black phosphorus and underlying mechanisms, Small 13 (32) (2017).
[32] P.D. Megaloikonomos, G.N. Panagopoulos, M. Bami, V.G. Igoumenou, L. Dimopoulos, A. Milonaki, M. Kyriakidou, E. Mitsiokapa, J. Anastassopoulou, A. F. Mavrogenis, Harvesting, isolation and differentiation of rat adipose-derived stem cells, Curr. Pharmaceut. Biotechnol. 19 (1) (2018) 19–29.
[33] Z. Sun, H. Xie, S. Tang, X.F. Yu, Z. Guo, J. Shao, H. Zhang, H. Huang, H. Wang, P. K. Chu, Ultrasmall black phosphorus quantum dots: synthesis and use as photothermal agents, Angew Chem. Int. Ed. Engl. 54 (39) (2015) 11526–11530.
[34] M. Morita, Y. Suyama, T. Notsu, K. Fukuoka, K. Ikuta, H. Kanayama, R. Umeda, S. Teraoka, H. Minato, H. Ninomiya, M. Tsuneto, Y. Shirayoshi, I. Hisatome, S. Yagi, Effects of conditioned medium of adipose-derived stem cells exposed to platelet-rich plasma on the expression of endothelial nitric oxide synthase and angiogenesis by endothelial cells, Ann. Plast. Surg. 90 (2) (2023) 171–179.
[35] S.J. Zhao, F.Q. Kong, J. Jie, Q. Li, H. Liu, A.D. Xu, Y.Q. Yang, B. Jiang, D.D. Wang, Z.Q. Zhou, P.Y. Tang, J. Chen, Q. Wang, Z. Zhou, Q. Chen, G.Y. Yin, H.W. Zhang, J. Fan, Macrophage MSR1 promotes BMSC osteogenic differentiation and M2-like polarization by activating PI3K/AKT/GSK3β/β-catenin pathway, Theranostics 10 (1) (2020) 17–35.
[36] S.J. Zhao, H. Liu, J. Chen, D.F. Qian, F.Q. Kong, J. Jie, G.Y. Yin, Q.Q. Li, J. Fan, Macrophage GIT1 contributes to bone regeneration by regulating inflammatory responses in an ERK/NRF2-Dependent way, J. Bone Miner. Res. 35 (10) (2020) 2015–2031.
[37] L. Wang, M. Lin, X. Hou, L. Dou, Z. Huang, R. Liu, J. Zhang, C. Cai, C. Chen, Y. Liu, D. Wang, D. Guo, R. An, L. Wei, Y. Yao, Y. Zhang, Black phosphorus quantum dots induce autophagy and apoptosis of human bronchial epithelial cells via endoplasmic reticulum stress, Chemosphere 327 (2023) 138463.
[38] F. Ruan, R. Liu, K. Wang, J. Zeng, Z. Zuo, C. He, Y. Zhang, Cytotoxicity of black phosphorus quantum dots on lung-derived cells and the underlying mechanisms, J. Hazard Mater. 402 (2021) 122875.
[39] Y. He, C. Yi, X.L. Zhang, W. Zhao, D.S. Yu, Magnetic graphene oxide: synthesis approaches, physicochemical characteristics, and biomedical applications, Trac. Trends Anal. Chem. 136 (2021).
[40] X. Mu, J.Y. Wang, X. Bai, F. Xu, H. Liu, J. Yang, Y. Jing, L. Liu, X. Xue, H. Dai, Q. Liu, Y.M. Sun, C. Liu, X.D. Zhang, Black phosphorus quantum dot induced oxidative stress and toxicity in living cells and mice, ACS Appl. Mater. Interfaces 9 (24) (2017) 20399–20409.
[41] J. Shao, H. Xie, H. Huang, Z. Li, Z. Sun, Y. Xu, Q. Xiao, X.F. Yu, Y. Zhao, H. Zhang, H. Wang, P.K. Chu, Biodegradable black phosphorus-based nanospheres for in vivo photothermal cancer therapy, Nat. Commun. 7 (2016) 12967.
[42] Y. He, Y. Li, G. Chen, C. Wei, X. Zhang, B. Zeng, C. Yi, C. Wang, D. Yu, Concentration-dependent cellular behavior and osteogenic differentiation effect induced in bone marrow mesenchymal stem cells treated with magnetic graphene oxide, J. Biomed. Mater. Res. 108 (1) (2020) 50–60.
[43] E. Canalis, Wnt signalling in osteoporosis: mechanisms and novel therapeutic approaches, Nat. Rev. Endocrinol. 9 (10) (2013) 575–583.
[44] J. Dai, Y. Li, H. Zhou, J. Chen, M. Chen, Z. Xiao, Genistein promotion of osteogenic differentiation through BMP2/SMAD5/RUNX2 signaling, Int. J. Biol. Sci. 9 (10) (2013) 1089–1098.
[45] C. Schlundt, H. Fischer, C.H. Bucher, C. Rendenbach, G.N. Duda, K. Schmidt-Bleek, The multifaceted roles of macrophages in bone regeneration: a story of polarization, activation and time, Acta Biomater. 133 (2021) 46–57.
[46] J. Pajarinen, T. Lin, E. Gibon, Y. Kohno, M. Maruyama, K. Nathan, L. Lu, Z. Yao, S. B. Goodman, Mesenchymal stem cell-macrophage crosstalk and bone healing, Biomaterials 196 (2019) 80–89.
[47] S.A. Eming, T.A. Wynn, P. Martin, Inflammation and metabolism in tissue repair and regeneration, Science 356 (6342) (2017) 1026–1030.
[48] A.C.R. Sridharan, D. Kelly, C. Kearney, F. O'Brien, Biomaterial based modulation of macrophage polarization: a review and suggested design principles, Mater. Today 18 (6) (2015) 313–325.
[49] C. Schlundt, T. El Khassawna, A. Serra, A. Dienelt, S. Wendler, H. Schell, N. van Rooijen, A. Radbruch, R. Lucius, S. Hartmann, G.N. Duda, K. Schmidt-Bleek,

Macrophages in bone fracture healing: their essential role in endochondral ossification, Bone 106 (2018) 78–89.
[50] S. Reinke, S. Geissler, W.R. Taylor, K. Schmidt-Bleek, K. Juelke, V. Schwachmeyer, M. Dahne, T. Hartwig, L. Akyüz, C. Meisel, N. Unterwalder, N.B. Singh, P. Reinke, N.P. Haas, H.D. Volk, G.N. Duda, Terminally differentiated CD8+ T cells negatively affect bone regeneration in humans, Sci. Transl. Med. 5 (177) (2013) 177ra36.
[51] K. Schmidt-Bleek, H. Schell, J. Lienau, N. Schulz, P. Hoff, M. Pfaff, G. Schmidt, C. Martin, C. Perka, F. Buttgereit, H.D. Volk, G. Duda, Initial immune reaction and angiogenesis in bone healing, J Tissue Eng Regen Med 8 (2) (2014) 120–130.
[52] A. Polymeri, W.V. Giannobile, D. Kaigler, Bone marrow stromal stem cells in tissue engineering and regenerative medicine, Horm. Metab. Res. 48 (11) (2016) 700–713.
[53] K. Zha, Y. Tian, A.C. Panayi, B. Mi, G. Liu, Recent advances in enhancement strategies for osteogenic differentiation of mesenchymal stem cells in bone tissue engineering, Front. Cell Dev. Biol. 10 (2022) 824812.
[54] C. Zhao, Y. Gu, Y. Wang, Q. Qin, T. Wang, M. Huang, H. Zhang, Y. Qu, J. Zhang, Z. Du, X.X. Jiang, L. Xu, miR-129-5p promotes osteogenic differentiation of BMSCs and bone regeneration via repressing Dkk3, Stem Cell. Int. 2021 (2021) 7435605.
[55] Y. Hu, Z. Wang, C. Fan, P. Gao, W. Wang, Y. Xie, Q. Xu, Human gingival mesenchymal stem cell-derived exosomes cross-regulate the Wnt/β-catenin and NF-κB signalling pathways in the periodontal inflammation microenvironment, J. Clin. Periodontol. 50 (6) (2023) 796–806.
[56] F. Diomede, G.D. Marconi, L. Fonticoli, J. Pizzicanella, I. Merciaro, P. Bramanti, E. Mazzon, O. Trubiani, Functional relationship between osteogenesis and angiogenesis in tissue regeneration, Int. J. Mol. Sci. 21 (9) (2020).
[57] A.P. Kusumbe, S.K. Ramasamy, R.H. Adams, Coupling of angiogenesis and osteogenesis by a specific vessel subtype in bone, Nature 507 (7492) (2014) 323–328.
[58] L.F. Tremble, M. McCabe, S.P. Walker, S. McCarthy, R.F. Tynan, S. Beecher, R. Werner, A.J.P. Clover, X.D.G. Power, P.F. Forde, C. Heffron, Differential association of CD68(+) and CD163(+) macrophages with macrophage enzymes, whole tumour gene expression and overall survival in advanced melanoma, Br. J. Cancer 123 (10) (2020) 1553–1561.
[59] Y. Xuan, L. Li, M. Ma, J. Cao, Z. Zhang, Hierarchical intrafibrillarly mineralized collagen membrane promotes guided bone regeneration and regulates M2 macrophage polarization, Front. Bioeng. Biotechnol. 9 (2021) 781268.
[60] M.L. Novak, T.J. Koh, Macrophage phenotypes during tissue repair, J. Leukoc. Biol. 93 (6) (2013) 875–881.
[61] G. Juban, B. Chazaud, Metabolic regulation of macrophages during tissue repair: insights from skeletal muscle regeneration, FEBS Lett. 591 (19) (2017) 3007–3021.
[62] M. Fu, J. Li, M. Liu, C. Yang, Q. Wang, H. Wang, B. Chen, Q. Fu, G. Sun, Sericin/nano-hydroxyapatite hydrogels based on graphene oxide for effective bone regeneration via immunomodulation and osteoinduction, Int. J. Nanomed. 18 (2023) 1875–1895.
[63] W. Peilin, P. Ying, W. Renyuan, L. Zhuoxuan, Y. Zhenwu, Z. Mai, S. Jianguo, Z. Hao, Y. Gang, L. Lin, L. Haodong, Size-dependent gold nanoparticles induce macrophage M2 polarization and promote intracellular clearance of Staphylococcus aureus to alleviate tissue infection, Mater Today Bio 21 (2023) 100700.